Evaluation of historical simulations in the HCLIM43-ALADIN regional climate downscaling ensemble over Europe in the EURO-CORDEX-CMIP6 framework

Grigory Nikulin[1,2], Peter Kuma[1,2], Fuxing Wang[1,2], Oskar Landgren[3], Aitor Aldama Campino[1,2], Bert van Ulft[4], Petter Lind[1,2], Andreas Dobler[3], Juan Carlos Sanchez[5], Joakim Löw[1], Michael Sahlin[1], Ole Bøssing Christensen[6], Fredrik Boberg[6], Patrick Samuelsson[1,2], and Carolina Nilsson[1]

[1]Swedish Meteorological and Hydrological Institute (SMHI), Norrköping, Sweden
[2]Bolin Centre for Climate Research, Stockholm University, Stockholm, Sweden
[3]Norwegian Meteorological Institute (MET Norway), Oslo, Norway
[4]Royal Netherlands Meteorological Institute (KNMI), De Bilt, The Netherlands
[5]Agencia Estatal de Meteorología (AEMET), Madrid, Spain
[6]Danish Meteorological Institute (DMI), Copenhagen, Denmark

Correspondence: Peter Kuma (peter.kuma@smhi.se)

Abstract. Regional climate downscaling has historically been complementary to global climate models, providing higher-resolution data for local-scale studies and climate services. We use the regional climate model HCLIM43-ALADIN to downscale six CMIP6 global models in eight simulations on a 12.5-km resolution European domain. This is the HCLIM community contribution to the EURO-CORDEX-CMIP6 multi-model downscaling ensemble involving several regional climate models and soon to be available publicly via the Earth System Grid Federation. We document the HCLIM43-ALADIN ensemble and evaluate the simulated results during the historical time period 1991–2020 against the gridded station observations E-OBS and the reanalyses CERRA, CERRA-Land, and ERA5, focusing on near-surface air temperature and precipitation. In winter in the global climate model-driven HCLIM simulations, a cold bias of about 3 °C and underestimated precipitation by about 25% are present in North Europe, and a warm bias of about 1 °C and overestimated precipitation of about 50% are present in Central and Southern Europe. In summer, a cold bias of about 1 °C and overestimated precipitation of about 25% are present in Northern Europe, and a warm bias of about 2 °C is present in Central and Southern Europe. Overestimated precipitation by about 200% is present in parts of Southern Europe, but this value is also amplified by the very low observed precipitation. Some of the temperature and precipitation biases are explainable by large-scale pressure field biases, causing a reduced westerly flow from the Atlantic. Positive temperature trends of about 0.5 °C per decade are present nearly everywhere and especially strong over Central and Eastern Europe (up to about 1.5 °C per decade in some regions and seasons). A comparison between the driving global models and downscaled simulations shows that the regional model tends to improve temperature biases but worsen precipitation biases. In our subjective choice of model ranking, the EC-Earth3-Veg-driven simulations are the best-performing, and the MIROC6-driven simulation is the worst-performing. Simulations of future climate scenarios until 2100 with HCLIM43-ALADIN will be analysed in a separate publication. The presented simulations can be used for decision-making and will contribute to planned multi-model EURO-CORDEX-CMIP6 analyses.

1 Introduction

Regional climate projections, which complement global climate projections, have become an essential source of high-resolution climate data with typical spatial resolutions ranging from a few to several tens of kilometres. They are crucial for assessing regional climate change and supporting adaptation planning at regional, national, and local scales. During the last 15 years, regional climate downscaling activities organised within the framework of the Coordinated Regional Climate Downscaling Experiment (CORDEX; Giorgi et al., 2009; Jones et al., 2011), supported by the World Climate Research Programme (WCRP), have achieved significant advances in producing and delivering ensembles of high-resolution regional climate projections worldwide (Diez-Sierra et al., 2022).

The first phase of CORDEX (approximately 2009–2020) focused on downscaling a subset of global climate models (GCMs) from the Coupled Model Intercomparison Project Phase 5 (CMIP5; Taylor et al., 2012). The CMIP5-driven CORDEX simulations are extensively applied worldwide to investigate global and regional drivers of climate change and to support numerous climate change assessments at regional (e.g. ESCWA, 2017), national (e.g. Hanssen-Bauer et al., 2015; MeteoSwiss and ETH Zurich, 2025) and local (e.g. Yeste et al., 2021) levels. Moreover, CORDEX-CMIP5 simulations have significantly contributed to major Intergovernmental Panel on Climate Change (IPCC) assessment reports, including the Special Report on Global Warming of 1.5 °C (SR1.5; Masson-Delmotte et al., 2018) and the Sixth Assessment Report (AR6; IPCC, 2023) and its interactive atlas (Gutiérrez et al., 2021), as well as the Copernicus Interactive Climate Atlas (Copernicus Climate Change Service (C3S), 2026). Current CORDEX activities from approximately 2020 onwards (Gutowski Jr. et al., 2016) focus on downscaling a subset of global models from CMIP Phase 6 (CMIP6; Eyring et al., 2016). Many regional modelling groups worldwide have been actively working on generating new CORDEX-CMIP6 simulations, contributing to the emerging continental-scale CORDEX-CMIP6 ensembles. A range of regional climate models (RCMs), developed by individual institutions and modelling communities, are used to create these ensembles, which in turn consist of sub-ensembles produced by single RCM members driven by multiple GCMs and reanalyses.

It is now well understood that, in general, higher resolution in global and regional climate modelling helps reduce systematic model biases, i.e., deviations of simulated climate from observations (e.g. Roberts et al., 2018; Ban et al., 2021). However, even high-resolution RCMs, like all models that approximate the Earth system, still exhibit errors when simulating the recent climate (e.g. Nikulin et al., 2012; Kotlarski et al., 2014; Wu et al., 2020; Vautard et al., 2021). These RCM biases arise both from internal structural limitations (e.g. parameterisation of complex physical processes, domain and resolution dependence and representation of land–atmosphere coupling) and from biases inherited through boundary conditions provided by the driving GCMs.

A common first step in analysing RCM ensembles is to conduct evaluation studies that aim to quantify, and where possible to understand, the various biases present in individual ensemble members. Such evaluation studies underpin the identification of the strengths and limitations of individual ensemble members, thus supporting the careful and scientifically rigorous use of RCM ensembles in climate research and other applications. Evaluation of CORDEX grand ensembles typically includes analysis of an evaluation experiment driven by reanalysis data, which are generally regarded as the most realistic boundary conditions available, even though they are also affected by biases (e.g. Hersbach et al., 2020). This approach enables the identification of structural RCM biases under idealised boundary conditions (Nikulin et al., 2012; Kotlarski et al., 2014). A further step involves evaluating RCM simulations driven by GCMs under historical conditions with prescribed observed forcings. This approach combined with analysis of the evaluation experiment allows the identification of RCM biases inherited from the driving GCMs (Rana et al., 2020).

Among the different regional domains under the CORDEX umbrella, the largest CORDEX-CMIP5 ensemble was generated under the EURO-CORDEX framework, employing 11 RCMs run by multiple partner institutions (Jacob et al., 2020; Vautard et al., 2021; Coppola et al., 2021) over the European domain. Among these, the Rossby Centre Regional Atmospheric Climate Model version 4 (RCA4; Samuelsson et al., 2015; Strandberg et al., 2015) and HIRHAM5 (Christensen et al., 2007b) models, maintained by the Swedish Meteorological and Hydrological Institute (SMHI) and the Danish Meteorological Institute (DMI), respectively, have been retired and are no longer used for the generation of regional climate projections. However, a new community regional modelling system, HCLIM (described in Section 2.1.1), jointly developed by several European partners, now contributes to the EURO-CORDEX-CMIP6 ensemble. HCLIM has its origins in the HARMONIE numerical weather prediction (NWP) system, used by several National Meteorological and Hydrological Services (NMHSs) in Europe for operational weather forecasting. Development of HCLIM began around a decade ago, and the system has since contributed to multiple research projects and CORDEX activities. However, this is the first time HCLIM contributes to the CORDEX continental-scale ensembles.

Adding a new RCM with no direct predecessor helps maintain model diversity in the EURO-CORDEX-CMIP6 ensemble after the retirement of RCA4 and HIRHAM5. Evaluating the new HCLIM43-ALADIN model within EURO-CORDEX constitutes a necessary and logical step for establishing a robust foundation for the use of the EURO-CORDEX-CMIP6 ensemble. In this study, we present an initial evaluation of the HCLIM ensemble produced for EURO-CORDEX, considering both the European Centre for Medium-Range Weather Forecasts (ECMWF) Reanalysis 5 (ERA5; Hersbach et al., 2020)-driven evaluation and CMIP6 GCM-driven historical simulations. The primary objectives of this study are to: i) present the HCLIM43-ALADIN model and its EURO-CORDEX-CMIP6 ensemble; ii) assess seasonal mean near-surface air temperature and precipitation biases in the HCLIM ensemble; and iii) establish a reference for the EURO-CORDEX HCLIM43-ALADIN ensemble.

2 Data and methods

2.1 Simulations

2.1.1 HCLIM regional modelling system

The High Resolution Limited Area Model (HIRLAM)–ALADIN Research on Mesoscale Operational numerical weather prediction in Euromed (HARMONIE)-Climate (HCLIM) is a seamless regional climate modelling framework. It is based on HARMONIE and developed by a consortium of European national meteorological institutes. It is jointly developed by several European partners: the Spanish State Meteorological Agency (AEMET), the Danish Meteorological Institute (DMI), the

Finnish Meteorological Institute (FMI), the Hungarian Meteorological Service (HungaroMet), the Royal Netherlands Meteorological Institute (KNMI), the Norwegian Meteorological Institute (METNo), the Irish Meteorological Service (Met Éireann), the Swedish Meteorological and Hydrological Institute (SMHI), and the Croatian Meteorological and Hydrological Service (DHMZ) as an associated member, in close collaboration with the A Consortium for Convection-scale modelling Research and Development (ACCORD) and the HIRLAM–ALADIN/United Weather Centers model development communities.

The HCLIM framework incorporates three NWP physics packages— the HARMONIE version of the Application of Research to Operations at Mesoscale (HARMONIE-AROME); Aire Limitée Adaptation Dynamique Développement International (ALADIN); and ALadin–AROme (ALARO). Each is optimised for use at different horizontal resolutions. AROME is optimised for convection-permitting scales (~1 km), ALARO for the 'grey zone' (~5 km), and ALADIN for coarser mesoscales (Termonia et al., 2018). Major HCLIM versions are referred to as cycles to maintain consistency with the corresponding NWP model configurations. The cycle numbering follows that of the global models Action de Recherche Petite Échelle Grande Échelle (ARPEGE) developed by Météo-France and Integrated Forecasting System (IFS) developed by the ECMWF (Buizza et al., 2018), from which the HARMONIE system is derived. The first HCLIM release corresponded to cycle 36 (Lindstedt et al., 2015; Lind et al., 2016), followed by cycles 38 (Belušić et al., 2020) and 43, the latter of which is used in CORDEX-CMIP6 and this study. Currently, cycle 46 is under active development in preparation for CORDEX-CMIP7. Proven effective in various simulations across different domains and resolutions (e.g. Belušić et al., 2020; Lind et al., 2020, 2023; Wu et al., 2020; Wang et al., 2023) and international collaborative projects (e.g. Coppola et al., 2020; Ban et al., 2021; Pichelli et al., 2021; Berthou et al., 2022; Médus et al., 2022; van Lipzig et al., 2022), HCLIM stands out as a robust regional climate modelling system.

The ALADIN physical package, used in its hydrostatic configuration, is applied in CORDEX simulations with grid spacings of approximately 10 km or coarser. It represents the limited-area version of the global model ARPEGE, from which it inherits its dynamical core and physical parameterisations (Termonia et al., 2018). The radiation scheme is a simplified version adapted from the ECMWF model (Mascart et al., 2009). Deep convection follows Bougeault (1985), turbulence is represented using the Cuxart–Bougeault–Redelsperger (CBR) scheme (Cuxart et al., 2000) with the mixing length formulation of Bougeault and Lacarrere (1989), and microphysics are based on Lopez (2002) and Bouteloup et al. (2005). The surface parameterisation framework in HCLIM is provided by the Surface externalisée (SURFEX) model (Masson et al., 2013), an externalised surface modelling system that can be used both in stand-alone (offline) mode and, in the case of HCLIM, coupled with an atmospheric model. Subgrid-scale surface heterogeneity is represented by four surface tiles: natural continental surfaces, sea, inland water, and urban areas. Urban surfaces are simulated using the Town Energy Balance (TEB) scheme (Masson, 2000), which is based on the Urban Canyon approach of Nunez and Oke (1977). Natural surfaces are parameterised with the Interactions Soil–Biosphere–Atmosphere (ISBA) model (Noilhan and Planton, 1989). Snow processes are represented by the 12-layer ISBA explicit snow (ISBA-ES) scheme (Boone, 2002). The Simple Ice (SICE) model (Batrak et al., 2018) is used for ocean surfaces, incorporating thermodynamically driven prognostic sea-ice thickness and snow (ISBA-ES) on sea ice, while sea-ice concentration and sea surface temperatures are updated from the boundary model at the same frequency as the lateral boundary conditions. Inland water is simulated by the lake model FLake (Mironov et al., 2010). In HCLIM43, SURFEX v8.1 is used together with land use data ECOCLIMAP Second Generation 300m (Druel et al., 2022), the sand/clay data SoilGrids250m version 2.0, and the orography data Global Multi-resolution Terrain Elevation Data 2010 (GMTED2010; Danielson and Gesch, 2011). A more thorough description of SURFEX v8.1 is given by Le Moigne et al. (2018).

2.1.2 Greenhouse gas and aerosol forcing

The HCLIM43 radiation scheme accounts for six greenhouse gases (GHGs): CO_2, CH_4, O_3, CFC-11, CFC-12, and N_2O. The global, annual-mean concentrations of five of these GHGs, CO_2, CH_4, CFC-11, CFC-12, and N_2O, are updated at each radiation time step by interpolating to the nearest monthly values. These GHG concentration time series for both the CMIP6 historical and scenario periods are available through the input4MIPs database (Meinshausen et al., 2017, 2020) and are provided by the ECMWF via the Radiation Scheme documentation (ECMWF, 2026a). For ozone (O_3), HCLIM43 uses a climatology derived from the Copernicus Atmosphere Monitoring Service (CAMS) data (Inness et al., 2019). In the ERA5-driven evaluation experiment, the model applies the CMIP6 historical atmospheric GHG forcing up to 2014. For the period from 2015 onwards (e.g., 2015–2020), HCLIM43 follows the CORDEX-CMIP6 experiment design and uses GHG concentrations under the shared socio-economic pathway 1-2.6 (SSP1-2.6; van Vuuren et al., 2017; Meinshausen et al., 2020).

HCLIM, in its default configuration, uses a monthly varying aerosol climatology for atmospheric optical depth (AOD) at 550 nm across five aerosol types. These five types include sea salt, dust, black carbon, organic aerosols, and sulphate aerosols. Organic and sulphate aerosols are combined and treated as a single aerosol class. This climatology is based on the monthly fields of Tegen et al. (1997) and follows the implementation used in the ECMWF IFS model (ECMWF, 2016). Using aerosol climatologies in RCMs leads to an underestimation of recent summer near-surface air temperature trends over Western and Eastern Europe (Boé et al., 2020; Nabat et al., 2025; Schumacher et al., 2024). This bias arises because the climatologies do not capture the substantial decline in aerosol load over Europe in recent decades (Schilliger et al., 2024). To address this aerosol-forcing issue, the EURO-CORDEX-CMIP6 experiment design requires all contributing RCMs to use transient aerosol forcing that includes both monthly and interannual variability (Katragkou et al., 2024).

For the CORDEX-CMIP6 ERA5-driven evaluation experiment, HCLIM43 uses monthly mean AOD 550 nm fields for the five aerosol types (as listed above) taken from the Modern-Era Retrospective Analysis for Research and Applications, Version 2 (MERRA2; Gelaro et al., 2017). For the CMIP6 GCM-driven simulations, monthly mean aerosol fields for the same five aerosol types are taken directly from the driving GCMs when all five types are available. However, several CMIP6 GCMs provide only total AOD rather than the five individual aerosol classes required by HCLIM43. To address this limitation, all CMIP6 GCMs that do provide the full set of aerosol classes for all four CMIP6 Tier 1 scenarios are utilised to compute ensemble-mean ratios between each aerosol-class AOD and the total AOD. This reference subset consists of eight models: NorESM2-MM, CNRM-ESM2-1, IPSL-CM6A-LR, MIROC6, GFDL-ESM4, GISS-E2-1-G, INM-CM5-0, and MRI-ESM2-0. These ensemble-mean ratios were then applied to decompose total AOD into the five required classes for the driving GCMs that provide only total AOD (EC-Earth3-Veg and MPI-ESM1-2-HR). Although not perfect, this approach is considered the best available approximation for constructing the aerosol forcing for EC-Earth3-Veg and MPI-ESM1-2-HR.

2.1.3 HCLIM43-ALADIN contribution to the EURO-CORDEX-CMIP6 ensemble

Nine CMIP6 GCMs were selected for downscaling in EURO-CORDEX-CMIP6 based on a number of criteria, including data availability, model plausibility, representation of future climate-change uncertainty, and model independence (Sobolowski et al., 2025). Three NMHSs—METNo, DMI, and SMHI—have downscaled six of the nine selected CMIP6 GCMs by applying HCLIM43-ALADIN over the EURO-CORDEX domain at a spatial resolution of 12.5 km (Table 1). These six GCMs encompass a broad range of climate sensitivities, with transient climate response (TCR) values spanning from the lower end of 1.33 (NorESM2-MM) to the upper end of 2.62 K (EC-Earth3-Veg).

In addition to downscaling a single realisation from each GCM, two additional EC-Earth3-Veg ensemble members initialised with different initial conditions were also downscaled. Together, these three HCLIM simulations, each driven by a distinct EC-Earth3-Veg realisation, enable an assessment of the role of internal climate variability in shaping future climate change signals. The CMIP variant labels are in the format r*k*i*l*p*m*f*n*, where *k* is the realisation index (initial conditions), *l* is the initialisation index (initialisation procedure), *m* is the physics index (physics version), and *n* is the forcing index (variants of forcing) (Taylor et al., 2025). When calculating ensemble means, only the first EC-Earth3-Veg realisation (r1i1p1f1) is included. This ensures that the HCLIM ensemble is not biased by the presence of multiple EC-Earth3-Veg-driven simulations.

All HCLIM43-ALADIN GCM-driven simulations are transient and were conducted for 1950–2100, with 1950–2014 driven by historical GCM simulations and 2015–2100 by future scenario simulations. To ensure a more effective model spin-up, the historical simulations were initialised on 1 August 1950, when Scandinavia is generally snow-free and lakes are ice-free. The ERA5-driven simulation was initialised on 1 August 1979 and spans the period 1980–2023. The first complete year of the historical runs (1951) and of the evaluation experiment (1980) is considered a spin-up year. To refer to the HCLIM simulations driven by the different GCMs and ERA5, we use the notation 'HCLIM(*driving model*)' in the text and 'HC(*driving model*)' in the figures.

2.2 Observations and reanalyses

A daily gridded observational dataset over Europe, E-OBS version 30.0e, at 0.1° spatial resolution (Cornes et al., 2018) is used as the primary reference for near-surface air temperature (tas) and precipitation (pr). The Copernicus European Regional Reanalysis (CERRA), which provides spatially and temporally consistent historical reconstructions of meteorological variables over Europe at 5.5-km resolution, is also utilised (Ridal et al., 2024). In CERRA, precipitation is entirely forecast-based, whereas CERRA-Land (Le Moigne et al., 2021) benefits from the assimilation of gauge-derived precipitation and has been demonstrated to outperform CERRA in reproducing precipitation. For this reason, CERRA is used in this study as an additional reference for temperature and CERRA-Land for precipitation. The ERA5 driving reanalysis (Hersbach et al., 2020) is also included in the evaluation and is used as the reference for sea-level pressure (SLP). All reference datasets are remapped to the Lambert Conformal Conic projection (LCC) used by HCLIM43-ALADIN. ERA5 is remapped from its native resolution of about 0.3° to 12.5 km using linear interpolation, whereas CERRA and CERRA-Land are aggregated from 5.5-km to the 12.5-km HCLIM LCC grid using a conservative remapping method.

Table 1. Driving CMIP6 GCMs, variant labels, and scenarios downscaled by HCLIM43-ALADIN, the institution which produced the downscaled simulation, the equilibrium climate sensitivity (ECS) and the transient climate response (TCR) of the driving GCM, and the institutions which produced the global simulation and references. The meaning of variant labels is described in the text.

Driving GCM	Variant	Scenarios (SSP)	RCM inst.	ECS (K)	TCR (K)	GCM inst. and references
CNRM-ESM2-1	r1i1p1f2	1-2.6, 3-7.0	SMHI	4.76	1.86	CNRM[i] and CERFACS[j] (Séférian et al., 2019)
EC-Earth3-Veg	r1i1p1f1	1-2.6, 3-7.0	SMHI	4.31	2.62	EC-Earth Consortium (Döscher et al., 2022)
EC-Earth3-Veg	r2i1p1f1	1-2.6, 3-7.0	SMHI	4.31	2.62	*the same as above*
EC-Earth3-Veg	r3i1p1f1	1-2.6, 3-7.0	SMHI	4.31	2.62	*the same as above*
IPSL-CM6A-LR	r1i1p1f1	1-2.6, 3-7.0	DMI	4.56	2.32	IPSL[k] (Boucher et al., 2020)
MIROC6	r1i1p1f1	1-2.6, 3-7.0	SMHI	2.61	1.55	JAMSTEC[b], AORI[c], NIES[d], and R-CCS[e] (Tatebe et al., 2019)
MPI-ESM1-2-HR	r1i1p1f1	1-2.6, 3-7.0	SMHI	2.98	1.66	MPI-M[f], DWD[g], and DKRZ[h] (Gutjahr et al., 2019)
NorESM2-MM	r1i1p1f1	1-2.6, 3-7.0, 5-8.5	METNo	2.50	1.33	NCC[a] (Seland et al., 2020)

[a]NorESM Climate modeling Consortium [b]Japan Agency for Marine-Earth Science and Technology [c]Atmosphere and Ocean Research Institute [d]National Institute for Environmental Studies [e]RIKEN Center for Computational Science [f]Max Planck Institute for Meteorology [g]Deutscher Wetterdienst [h]Deutsches Klimarechenzentrum [i]Centre National de Recherches Meteorologiques [j]Centre Europeen de Recherche et de Formation Avancee en Calcul Scientifique [k]Institut Pierre Simon Laplace

The 1991–2020 period is used for the evaluation. The World Meteorological Organization (WMO) defines this interval as the reference climatological period for the 2021–2030 decade (WMO, 2015), and it is the standard currently applied by NMHSs worldwide. Because the historical experiment is only available until 2014, in the GCMs and RCMs we use a composition of the CMIP6 historical experiment for 1991–2014 and the SSP1-2.6 scenario for 2015–2020. Given that the time period between 2015 and 2020 is short and very similar between the SSP scenarios, the choice of the scenario likely has a negligible impact on our results, other than through natural variability. Four canonical seasons are used in the study: December–February (DJF), March–May (MAM), June–August (JJA), and September–November (SON), along with the annual mean (ANN).

2.3 Statistical methods

To evaluate the HCLIM ensemble across European regions with contrasting climate conditions, eight subdomains defined within the PRUDENCE project (Christensen et al., 2007a; Christensen and Christensen, 2007) are used: the Alps (AL), the British Isles (BI), Eastern Europe (EA), France (FR), the Iberian Peninsula (IP), the Mediterranean (MD), Mid-Europe (ME), and Scandinavia (SC). Although these PRUDENCE regions are defined in a relatively simple manner and therefore do not perfectly represent homogeneous climate zones, they have been widely adopted in Europe climate model evaluation and climate change assessments because of their simplicity and consistency.

Seasonal and annual means are calculated as means for every year, and then an overall mean is calculated from this annual time series. December of the year $y-1$ is considered to be part of the winter season (December–January–February) of year y. Geographical means are calculated as weighted means taking into account the grid cell area. The ensemble mean of the GCM-driven HCLIM simulations is calculated as a simple mean of the ensemble members. The statistical significance of the simulation biases (Section 3.1 and 3.2) is determined using a two-sided t-test, as implemented by the SciPy library (Virtanen et al., 2020, function *ttest_rel*). The input time series to the test are 30 annual values (one value per year of the analysed 30-year time period) for both the simulation and the reference. Any trends during the period are not compensated for in the test. A paired t-test is used for comparing the reanalyses with observations, and an unpaired t-test is used for comparing the simulations with observations. All significance levels shown in the results (Section 3) use a 0.05 p-value threshold. The trends (Section 3.3) are calculated per grid cell using linear regression, and the significance is determined using the Wald Test with the t-distribution of the test statistic, as implemented by SciPy (function *linregress*).

In the plots (Fig. 1–8 and S1), values of near-surface air temperature and precipitation below the 2nd and 15th percentiles (respectively) and above the 98th and 85th percentiles (respectively) are shown outside the scale range. Precipitation anomalies in Fig. 3, 4, and 6 are shown as a fractional difference from the reference, $(R-R_{\text{obs}})/R_{\text{obs}}$, where R is the simulation or reanalysis precipitation rate and R_{obs} is the observed precipitation rate. To show the anomalies, we use logarithmic scale because the anomalies are bounded for low values by −100% and unbouded for high values, resulting in an uneven distribution around zero. The colour map scales are chosen so that they are symmetric and regular on the logarithmic scale $\log[(R-R_{\text{obs}})/R_{\text{obs}}]$.

2.4 Model ranking

The model ranking (Section 3.5) is calculated based on the simulation bias in the mean and standard deviation of daily mean, minimum, and maximum near-surface air temperature, precipitation, and SLP. The biases are determined relative to E-OBS over the entire reference period, except for SLP, which is relative to ERA5. The calculation of ranks is performed as follows. The variable mean $\bar{x}_{i,j,k,l}$ and standard deviation $s_{x_{i,j,k,l}}$ are calculated for the simulation i and variable j, over the area of the region k, and season l. Elemental simulation ranks for mean $\text{rank}(\bar{x}_{i,j,k,l})$ and standard deviation $\text{rank}(s_{x_{i,j,k,l}})$ are calculated based on the absolute difference between the simulation mean and the reference mean $|\bar{x}_{i,j,k,l}-\bar{x}^{\text{ref}}_{i,j,k,l}|$ and the absolute difference between the simulation standard deviation and the reference standard deviation $|s_{x_{i,j,k,l}}-s^{\text{ref}}_{x_{i,j,k,l}}|$, respectively. The elemental ranks are integers between 1 and 7 (the number of HCLIM simulations, including only the r1 variant of EC-Earth3-Veg), where 1 is the best rank (closest to the reference) and 7 is the worst (the furthest from the reference). The total rank rank_i, per-variable rank $\text{rank}_{i,j}$, and per-region rank $\text{rank}_{i,k}$ are calculated by averaging the elemental ranks of both the mean and standard deviation as

$$\text{rank}_i = \frac{1}{2n_j n_k n_l} \sum_{j,k,l} \left[\text{rank}(\bar{x}_{i,j,k,l}) + \text{rank}(s_{x_{i,j,k,l}})\right], \tag{1}$$

$$\text{rank}_{i,j} = \frac{1}{2n_k n_l} \sum_{k,l} \left[\text{rank}(\bar{x}_{i,j,k,l}) + \text{rank}(s_{x_{i,j,k,l}})\right], \tag{2}$$

$$\text{rank}_{i,k} = \frac{1}{2n_j n_l} \sum_{j,l} \left[\text{rank}(\bar{x}_{i,j,k,l}) + \text{rank}(s_{x_{i,j,k,l}})\right], \tag{3}$$

where n_j, n_k, and n_l are the number variables, regions, and seasons, respectively.

3 Results

3.1 Spatial distribution of biases

3.1.1 Temperature

Winter mean near-surface air temperature from E-OBS (Fig. 1a) exhibits a pronounced meridional gradient, spanning approximately 25 °C from around −10 °C in northern Scandinavia to about 15 °C in North Africa. In addition, a clear zonal gradient is evident, reflecting the transition from the maritime climate of Western Europe to the more continental conditions over Eastern Europe and Russia. Both CERRA and ERA5 show overall good agreement with E-OBS (Fig. 1b and c). ERA5 exhibits a weak, continent-wide warm bias, with the largest values (up to 3 °C) over northern Fennoscandia. In contrast, a cold bias is apparent over the Alpine region, the coast of Norway and the Kola Peninsula in ERA5. CERRA generally displays smaller, more regionally confined biases but tends to underestimate temperatures in southern Europe (up to 2 °C over the Iberian Peninsula) and over parts of Norway, where negative biases locally approach 3 °C. The HCLIM simulation driven by ERA5 (Fig. 1d) exhibits a widespread cold bias across much of the continent, with the largest negative deviations (up to 3 °C) over the Iberian and Appenine Peninsulas, Norway, and northeastern Europe. In contrast, simulated winter temperatures are in good agreement with E-OBS over Western Europe, including Germany, the Benelux, France, and the British Isles. This contrast between HCLIM(ERA5) and ERA5 shows that the internal dynamics and physics of HCLIM can substantially override the driving model in its near-surface air temperature.

The winter GCM-driven simulations (Fig. 1e–m) exhibit substantially larger biases relative to E-OBS compared to the ERA5-driven experiment. A consistent feature across all GCM-driven runs is a pronounced cold bias over Scandinavia and the eastern part of the EURO-CORDEX domain. This systematic pattern is also evident in their ensemble mean. The strongest cold bias, reaching up to 6 °C is found in HCLIM(MIROC6) (Fig. 1h), particularly over the eastern part of the domain. The other GCM-driven HCLIM simulations also exhibit substantial negative biases, generally underestimating winter mean temperatures by around 4 °C in Scandinavia. The smallest cold bias over Scandinavia is seen in the simulations driven by EC-Earth3-Veg (r1 and r2; Fig. 1k and l). The HCLIM simulation driven by NorESM2-MM (Fig. 1j) exhibits a pronounced warm bias across Western, Central, and Eastern Europe. In contrast, the other GCM-driven simulations except for the MIROC6-driven run show

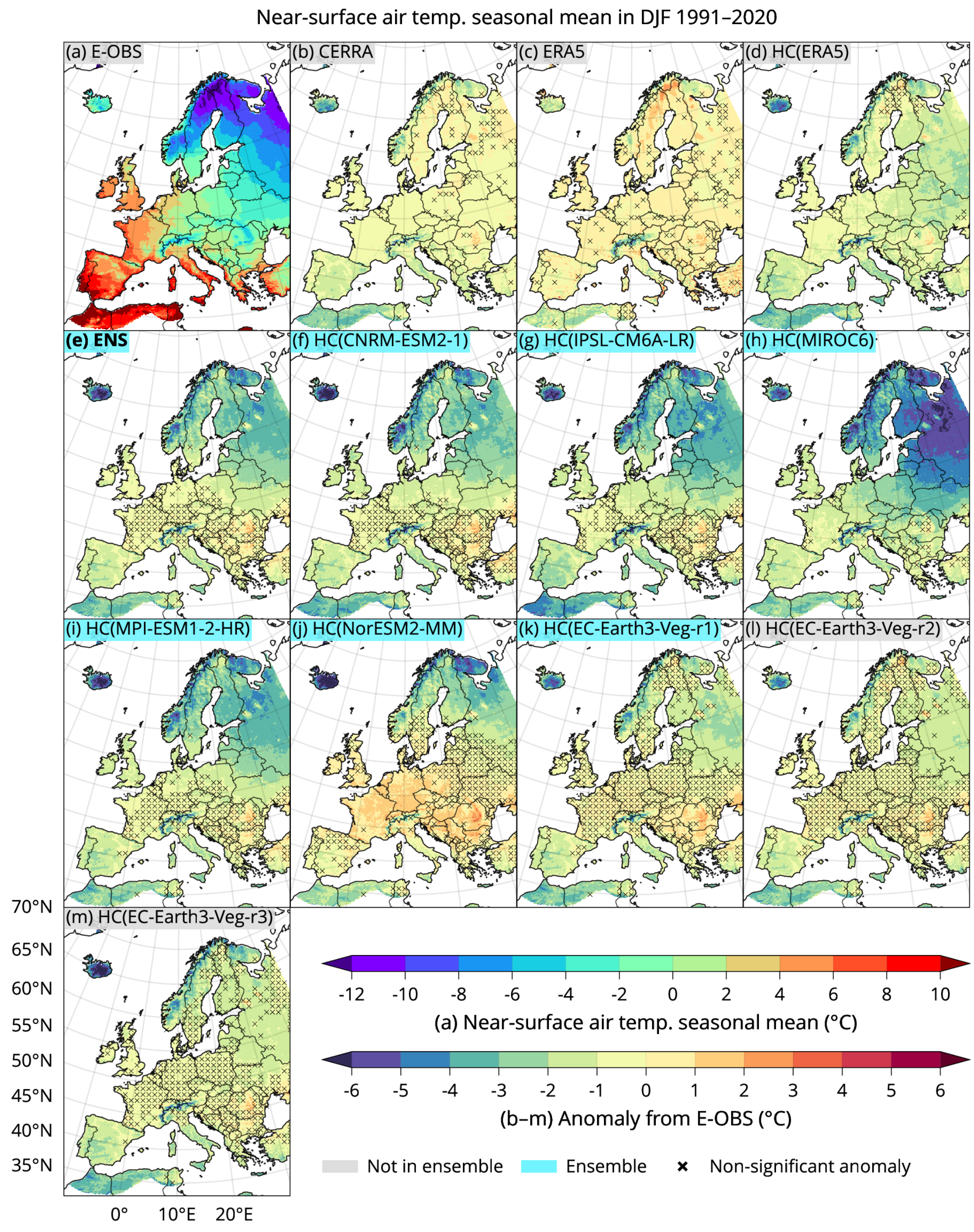

Figure 1. **(a)** E-OBS mean winter near-surface air temperature for 1991–2020 and differences compared to E-OBS in the **(b)** CERRA and **(c)** ERA5 reanalyses, **(d)** HCLIM driven by ERA5, **(e)** the ensemble mean of all of the HCLIM GCM-driven simulations highlighted in turquoise, and **(f–m)** the individual HCLIM simulations driven by each GCM. Areas of statistically non-significant biases are marked with crosses.

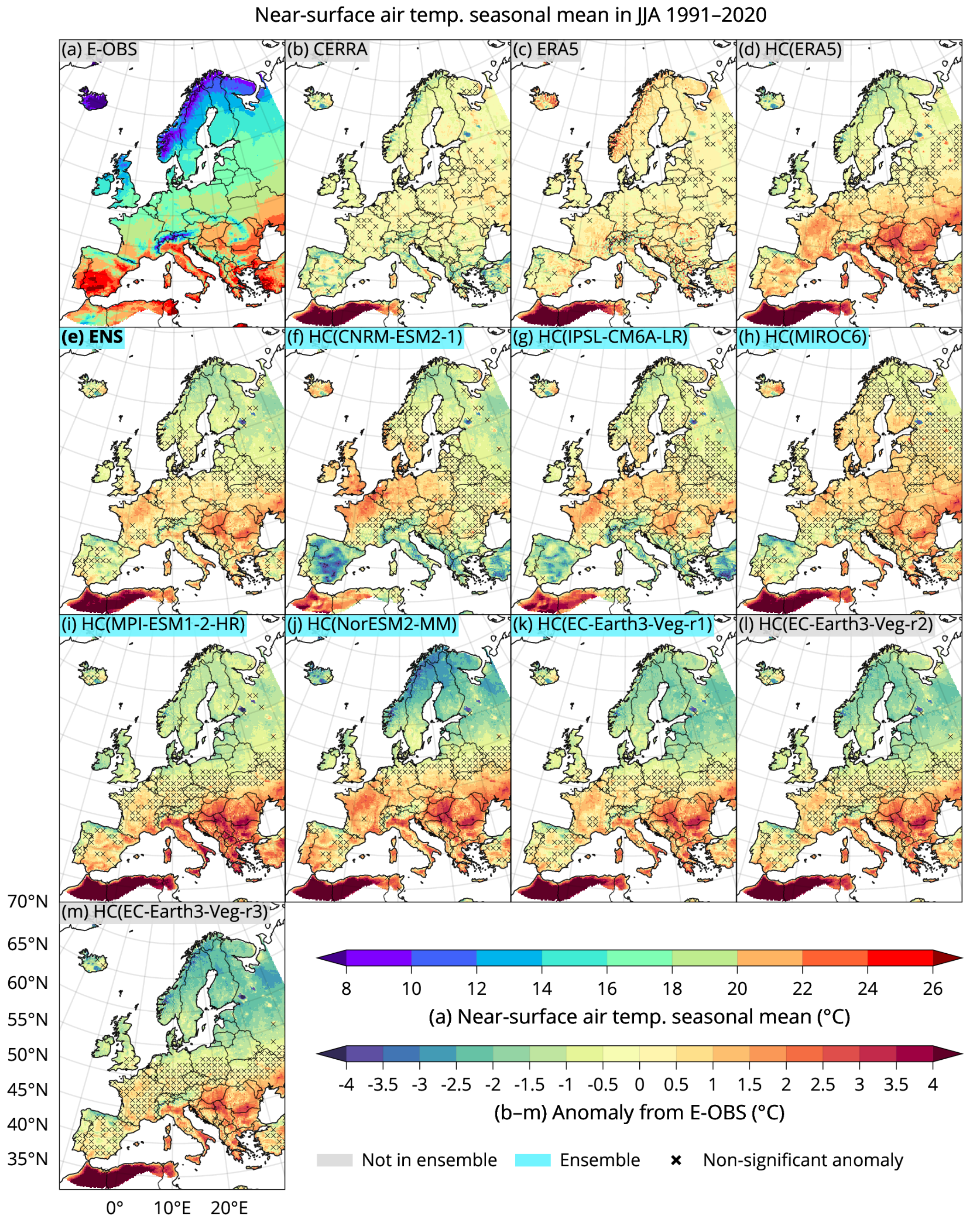

Figure 2. The same as Fig. 1 but for summer.

a more moderate warm bias west of the Black Sea, primarily over Bulgaria and Romania. The three ensemble members driven by EC-Earth3-Veg (Fig. 1k–m) display very similar bias patterns in both spatial distribution and magnitude. However, the third member is slightly colder overall, illustrating the influence of natural variability on the simulated mean winter temperature for 1991–2020.

Summer mean near-surface air temperature (Fig. 2a) has a smaller range over the domain compared to winter. The range is about 20 °C, ranging from about 8 °C over Scandinavia (Norway) to almost 30 °C in Southern Europe and North Africa. Similar to winter, both CERRA and ERA5 (Fig. 2b and c) have overall good agreement with E-OBS, and ERA5 is slightly warmer than E-OBS. The ERA5-driven simulation (Fig. 2c) exhibits a dipole bias pattern, characterised by a slight cold bias over Scandinavia and a more pronounced warm bias across central and Southern Europe. A similar pattern appears in the HCLIM simulations driven by NorESM2-MM, MPI-ESM2-HR, and EC-Earth3-Veg (Fig. 2j, i, and k–m), while those driven by CNRM-ESM2-1 and IPSL-CM6A-LR (Fig. 2f and g) show a negative bias over Southern Europe. The three members of the HCLIM(EC-Earth3-Veg) (Fig. 2k–m) ensemble exhibit nearly identical bias patterns and magnitudes, suggesting that internal variability in the simulated near-surface summer temperature is small. As in winter, the MIROC6-driven simulation (Fig. 2h) exhibits a bias pattern distinct from the other simulations, characterised by a positive bias of up to 3 °C over Eastern Europe.

3.1.2 Precipitation

Winter mean precipitation (Fig. 3a) reflects the influence of westerly flow from the Atlantic, resulting in generally wetter maritime climates near the coast and drier continental conditions farther inland. Orographic effects from mountain ranges such as the Scandinavian Mountains and Dinaric Alps further shape the precipitation distribution, with enhanced precipitation on the windward side and reduced precipitation on the leeward side. CERRA-Land (Fig. 3b), which assimilates gauge-based precipitation, agrees well with E-OBS over Western Europe and Scandinavia, although a small wet bias appears in the eastern part of the domain. In contrast, ERA5 (Fig. 3c), where precipitation is a purely prognostic variable, shows a widespread wet bias, reaching more than 80% in Eastern Europe. The HCLIM ERA5-driven evaluation simulation (Fig. 3d) reproduces a very similar bias pattern as ERA5. The GCM-driven simulations (Fig. 3e–m) substantially overestimate winter precipitation over mainland Europe while showing moderate dry biases over the Apennine Peninsula. In Scandinavia, they generally produce wetter conditions than E-OBS, although the spatial bias patterns differ among simulations. All simulations exhibit a dry bias on the windward side of the Scandinavian Mountains. The three members of the EC-Earth3-Veg-driven ensemble (Fig. 3k–m) show nearly identical bias patterns and magnitudes.

Summer mean precipitation (Fig. 4a) exhibits a markedly different spatial pattern from winter. While winter precipitation is largely controlled by Atlantic westerlies and large-scale precipitation from fronts and low pressure systems, summer precipitation is more strongly influenced by smaller scale convective processes. The Alps and the Carpathians are particularly wet during summer. As in winter, CERRA-Land (Fig. 4b) agrees well with E-OBS over Scandinavia and parts of Western Europe (e.g., Germany, the Benelux, and France). Elsewhere, a wet bias in the reanalyses is evident, with precipitation overestimated by more than 80% in parts of the Apennine Peninsula, Romania, the Balkans, and the Iberian Peninsula. ERA5 (Fig. 4c) shows a bias pattern broadly similar to that of CERRA-Land, with a small wet bias over Scandinavia and parts of Western Europe,

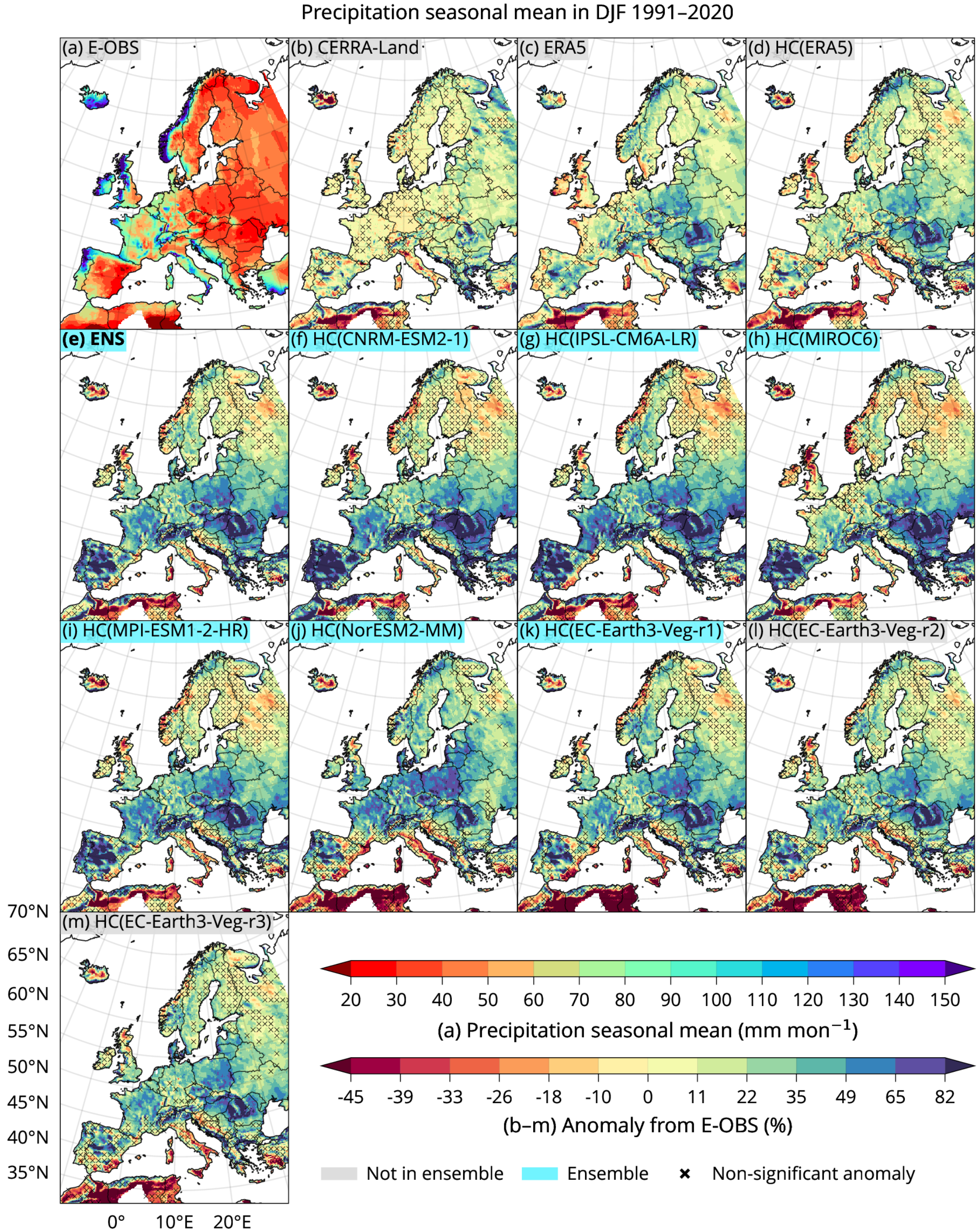

Figure 3. The same as Fig. 1 but for precipitation in winter and fractional difference (%). The precipitation anomaly colour scale is symmetric and regular on the logarithmic scale, as described in Section 2.3.

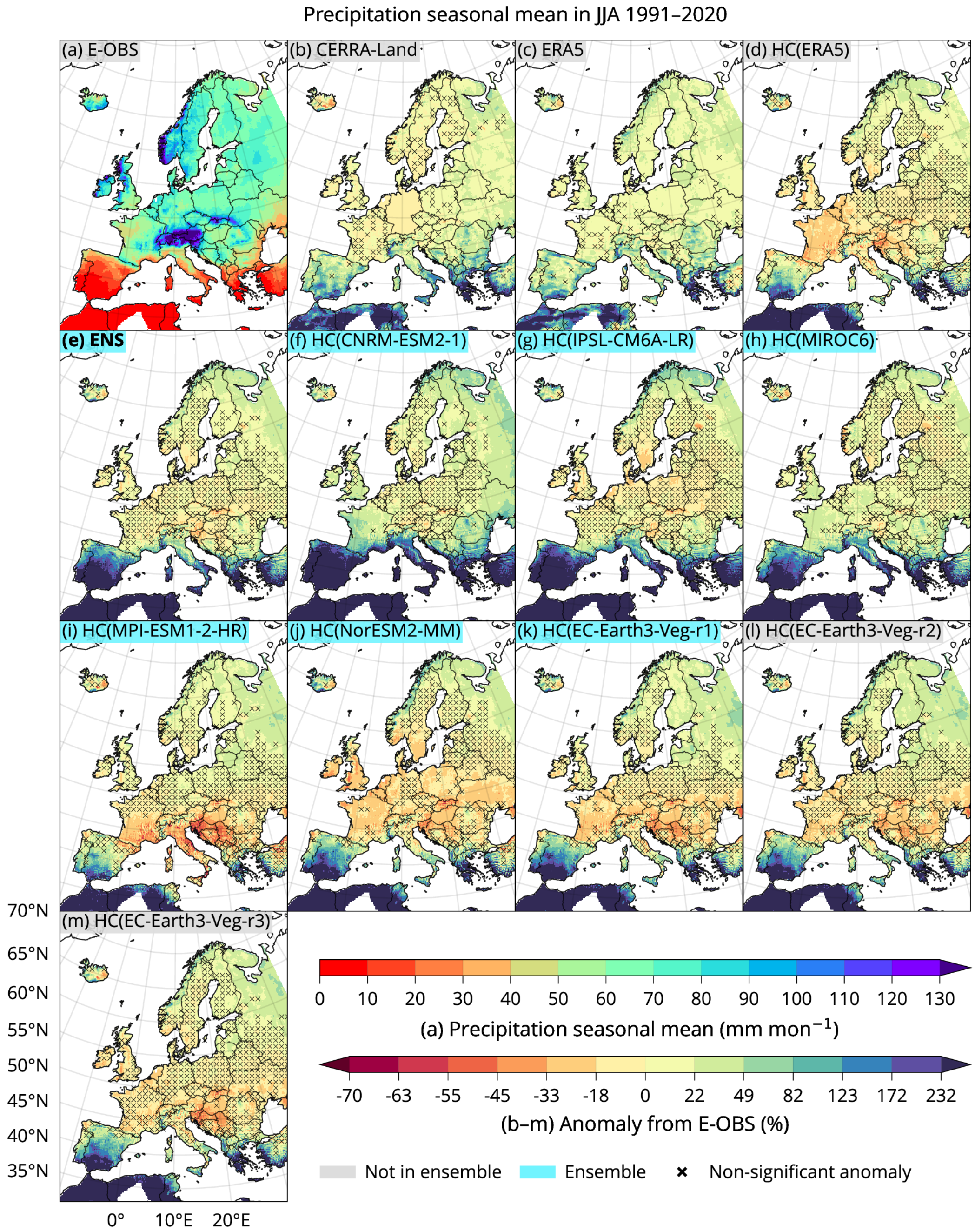

Figure 4. The same as Fig. 3 but for precipitation in summer.

where CERRA-Land exhibits almost no bias. The HCLIM(ERA5) simulation (Fig. 4d) underestimates summer precipitation in Western and parts of Eastern Europe, while overestimating it in northern Scandinavia and the southern Balkans.

There is no consistent bias pattern across the GCM-driven simulations, although smaller sub-ensembles can exhibit some similarities. The three simulations driven by CNRM-ESM2-1, MIROC6 and IPSL-CM6A-LR (Fig. 4f, h, and g) strongly overestimate precipitation over dry regions in Southern Europe and northern Mediterranean. Two of these three simulations (driven by CNRM-ESM2-1 and IPSL-CM6A-LR) also show a cold bias in summertime temperature over the same region (Fig. 2f and g) that may be related to the overestimation of precipitation. The MIROC6-driven simulation (Fig. 4h), however, does not show a similar cold bias. The simulations driven by MPI-ESM2-1-HR, NorESM2-MM, and EC-Earth3-Veg (Fig. 4i–m) have similar bias patterns with a wet bias over the northeastern parts of Europe and a dry bias in Southern and Central Europe. The dry bias is more pronounced in the NorESM2-MM-driven run, where the dry bias is stretching from Western to Eastern Europe. A common feature across all simulations is a wet bias in the northern part of the domain, although spatial details are different across the simulations.

3.2 Regional biases

3.2.1 Temperature

To further evaluate near-surface air temperature and precipitation biases in the HCLIM ensemble, Fig. 5 and 6 present seasonal and annual mean biases averaged over the PRUDENCE regions. CERRA exhibits predominantly small negative temperature biases, generally in the range of −1 to 0 °C across all PRUDENCE regions. In contrast, ERA5 shows small positive biases, typically below 1 °C. The HCLIM simulation driven by ERA5 largely changes the warm biases in ERA5 into negative biases across most seasons and PRUDENCE regions. In summer, however, the warm biases are amplified, except over the British Isles and Scandinavia, where they are negative. The individual GCM-driven simulations exhibit mixed biases across the seasons and PRUDENCE regions, with a tendency toward negative biases in winter, spring and autumn, and positive biases in summer. The simulations driven by CNRM-ESM2-1, IPSL-CM6A-LR, MIROC6, and MPI-ESM1-2-HR show pronounced cold biases, with strong underestimation of temperature over Scandinavia in winter, the Iberian Peninsula in spring and autumn, and the Alps in spring. These cold biases are also evident in the ensemble mean. The largest negative bias in the HCLIM simulation driven by MIROC6 reaches −3.7 °C over Scandinavia in winter, consistent with the spatial winter bias pattern shown in Fig. 1h. The HCLIM simulations driven by MIROC6, MPI-ESM1-2-HR, NorESM2-MM, and all members of EC-Earth3-Veg exhibit pronounced warm biases over the Mediterranean in summer. The largest warm bias (2.6 °C) occurs in the HCLIM simulation driven by MPI-ESM1-2-HR. These simulations consistently show substantial warm biases across southeastern Europe (see Fig. 2).

3.2.2 Precipitation

CERRA-Land and ERA5 show a slightly wetter climatology than E-OBS (Fig. 6). The HCLIM simulation driven by ERA5 exhibits precipitation biases that closely resemble those in ERA5, but with some regional and seasonal reversals in sign,

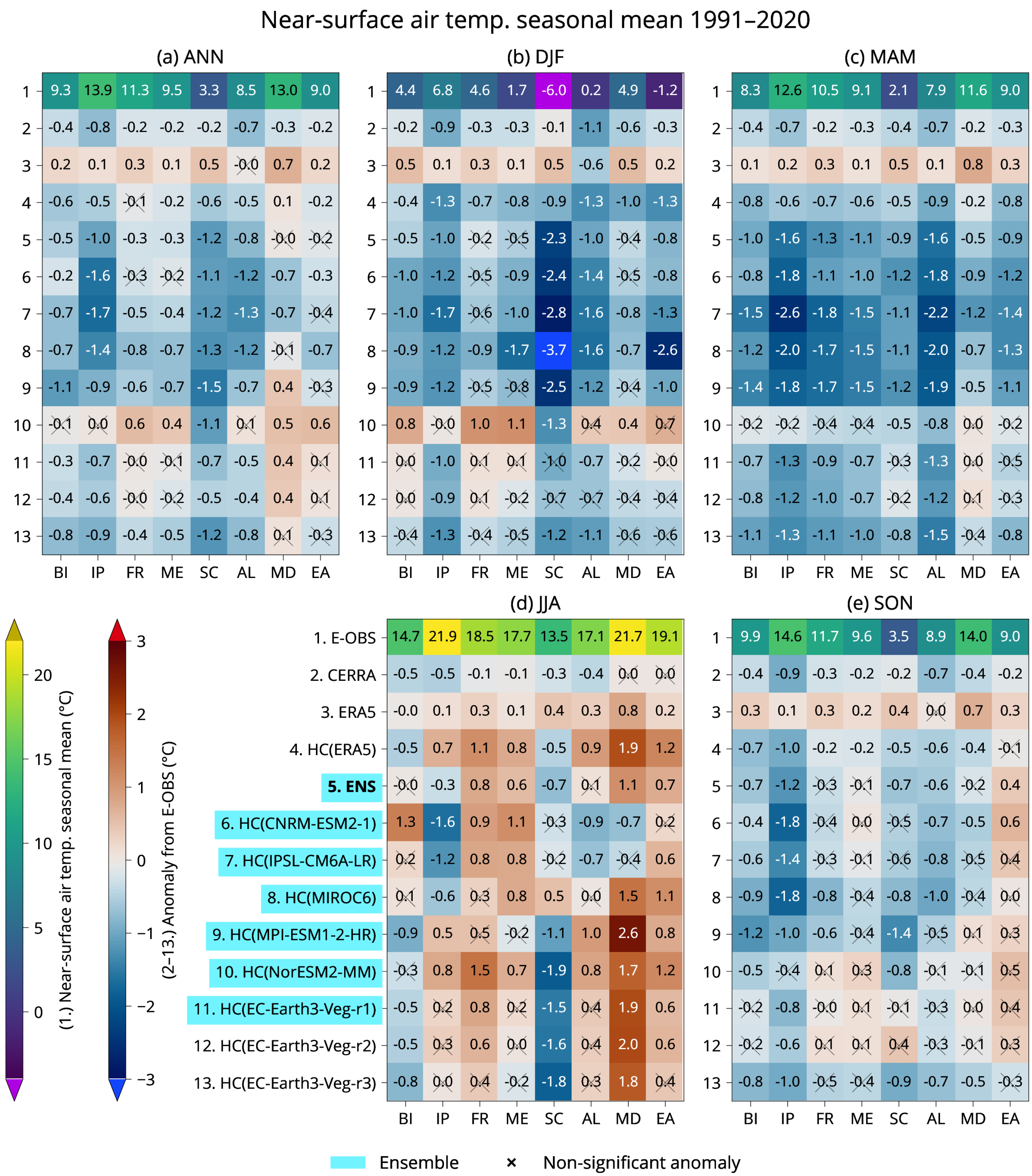

Figure 5. (Row 1) E-OBS near-surface air temperature for 1991–2020 averaged over the PRUDENCE regions and differences compared to E-OBS in the **(Row 2)** CERRA and **(Row 3)** ERA5 reanalyses, **(Row 4)** HCLIM driven by ERA5, **(Row 5)** the ensemble mean of all of the HCLIM GCM-driven simulations highlighted in turquoise and **(Row 6–13)** the individual HCLIM simulations driven by each GCM. Non-significant biases are marked with a cross.

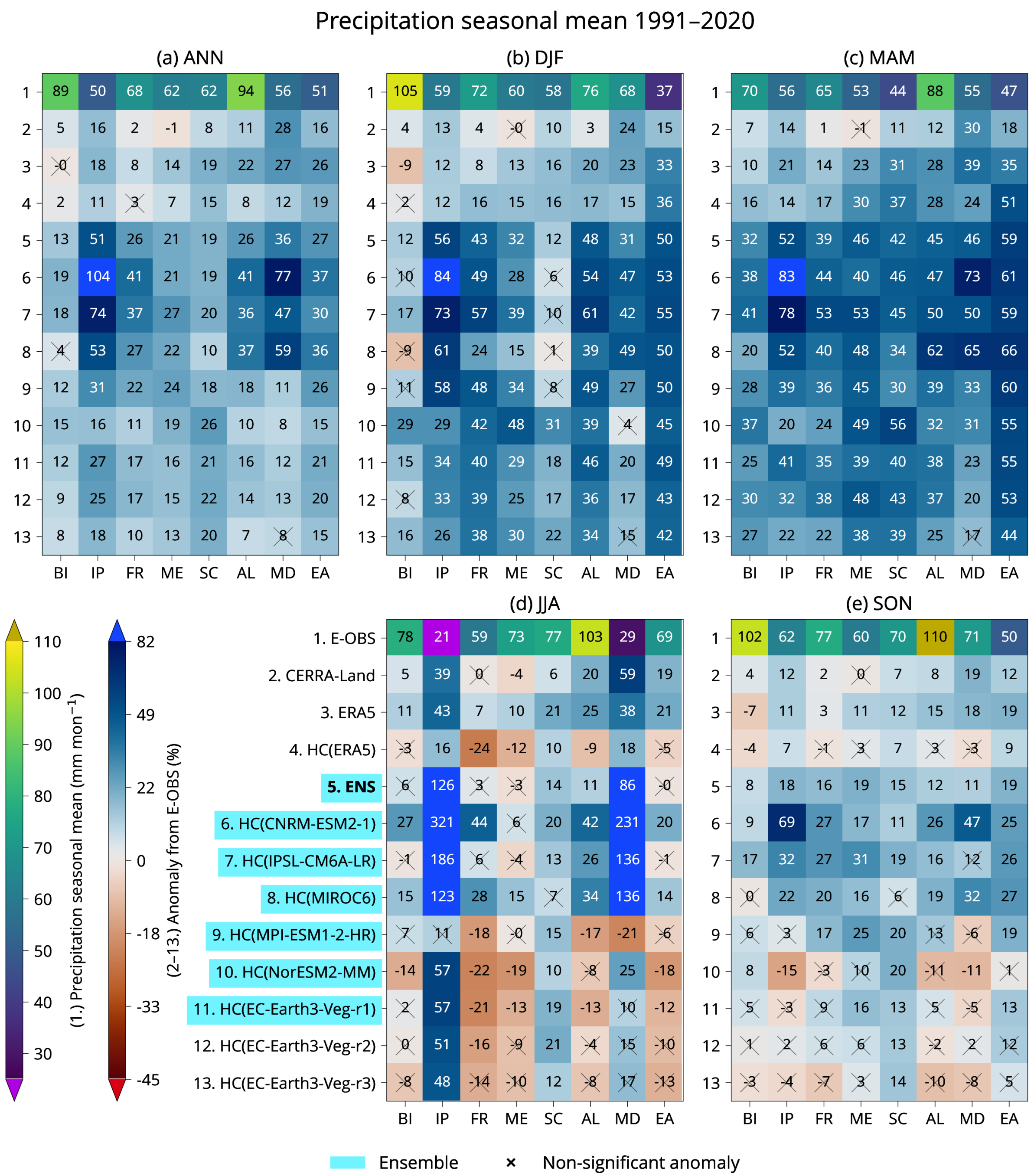

Figure 6. The same as Fig. 5 but for precipitation and fractional difference.

notably, for example, in summer over France, Mid-Europe, and the Alps. The GCM-driven simulations generally exhibit wet biases across all seasons and PRUDENCE regions, with some exceptions in summer when dry biases occur; however, most of these dry biases are not statistically significant. The Alpine region is consistently too wet in all GCM-driven simulations during winter. In summer, three HCLIM simulations driven by CNRM-ESM2-1, IPSL-CM6A-LR, and MIROC6 markedly overestimate precipitation over dry regions such as the Iberian Peninsula and the Mediterranean; this wet bias is also reflected in the ensemble mean. The strongest overestimation is found in the HCLIM(CNRM-ESM2-1) simulation. On average, the three members of the EC-Earth3-Veg–driven ensemble exhibit similar biases.

3.3 Trends in temperature

3.3.1 Spatial distribution of trends

The ability of climate models to accurately reproduce observed regional patterns of temperature and precipitation trends is an important measure for evaluating climate model performance. Schumacher et al. (2024) show that both CMIP6 and, in particular, CORDEX-CMIP5 ensembles underestimate the observed summer warming across much of Western and Central Europe over the period 1980–2022. This underestimation of recent observed temperature trends is attributed to the fact that simulated circulation changes are weaker than those in ERA5. In addition, most EURO-CORDEX regional climate models used in CORDEX-CMIP5 do not adequately capture local thermodynamic forcing associated with declining aerosol concentrations, as they typically have employed static aerosol forcing.

Observed and simulated winter near-surface air temperature trends for 1991–2020 are shown in Fig. 7. The E-OBS dataset is not homogenised and is therefore generally not recommended for trend analysis (Hofstra et al., 2009; van der Schrier et al., 2013). However, it is retained here to ensure consistency (Fig. 7a). In addition, the CERRA and ERA5 reanalyses (Fig. 7b and c) provide complementary estimates of observed trends, helping to better quantify associated uncertainties. Temperature trends for short time periods can be highly affected by natural variability. For the 30-year period 1991–2020, this is expected to be even more important than for the circulation changes during the 43-year period used by Schumacher et al. (2024). However, using the three EC-Earth3-Veg HCLIM simulations enables us to assess the role of the natural variability to a certain degree.

It should be noted that winter temperature trends for 1991–2020 are statistically non-significant at the grid-point level across most of the EURO-CORDEX domain (Fig. 7a–c). Significant trends are detected only in parts of Southern Europe. This is most likely attributable to the large interannual variability in winter temperatures, which can obscure underlying temperature trend estimates, particularly at regional and seasonal scales. However, aggregating the data to annual mean temperatures substantially reduces the influence of the variability and reveals statistically significant warming trends across all of Europe (Fig. S1). In practice, seasonal mean temperature trends are in general more relevant for national, regional, and local climate change assessments, as annual mean trends tend to smooth out important seasonal differences that are critical for many climate-sensitive sectors.

In winter, E-OBS, CERRA and ERA5 show similar large-scale patterns in near-surface temperature trends, with the strongest warming (up to 1°C per decade) occurring over Central and Eastern Europe and northwestern parts of Russia (Fig. 7a–c).

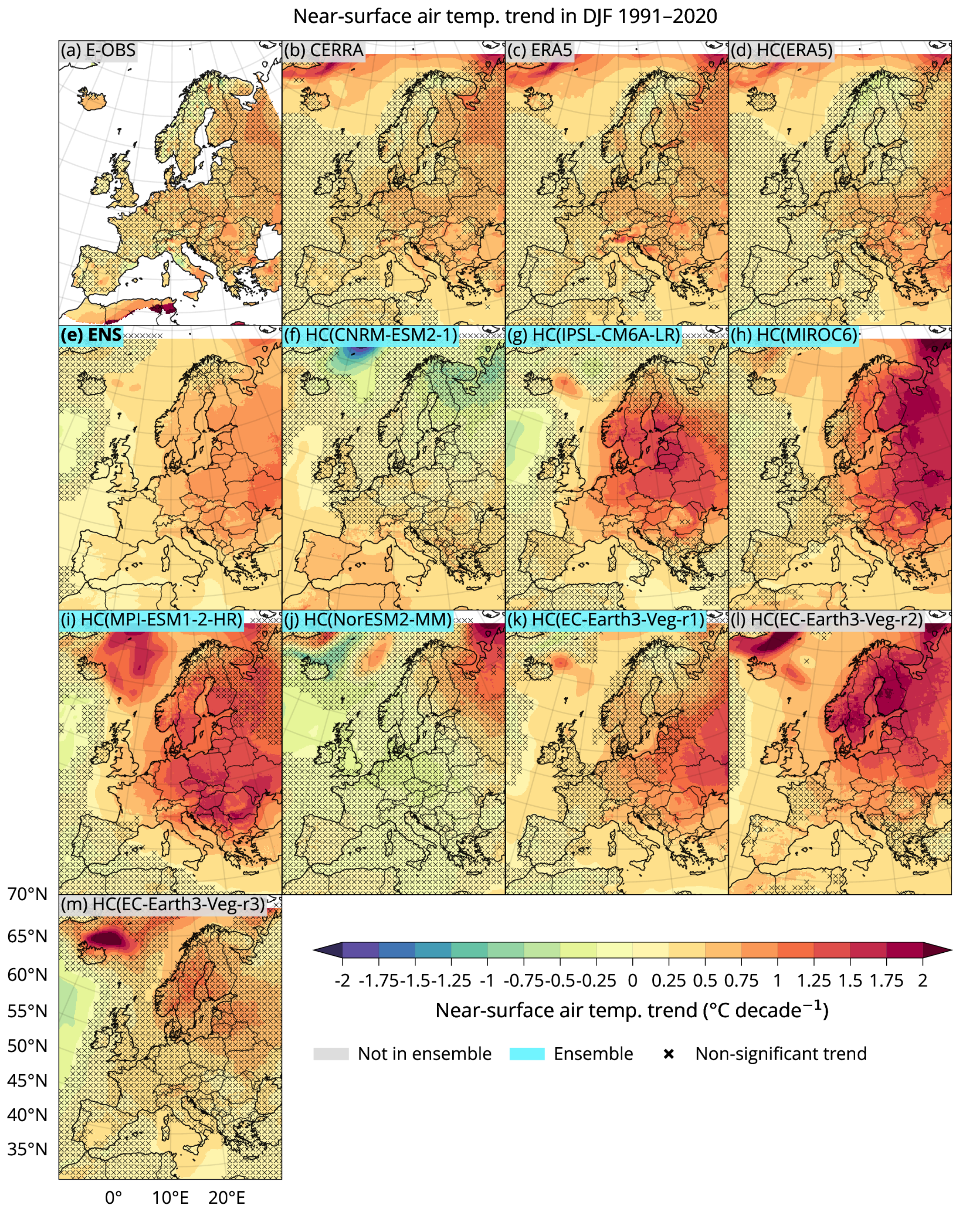

Figure 7. The same as Fig. 1 but for the linear trend of winter mean near-surface air temperature in 1991–2020 (°C per decade). Non-significant trends are marked with a cross.

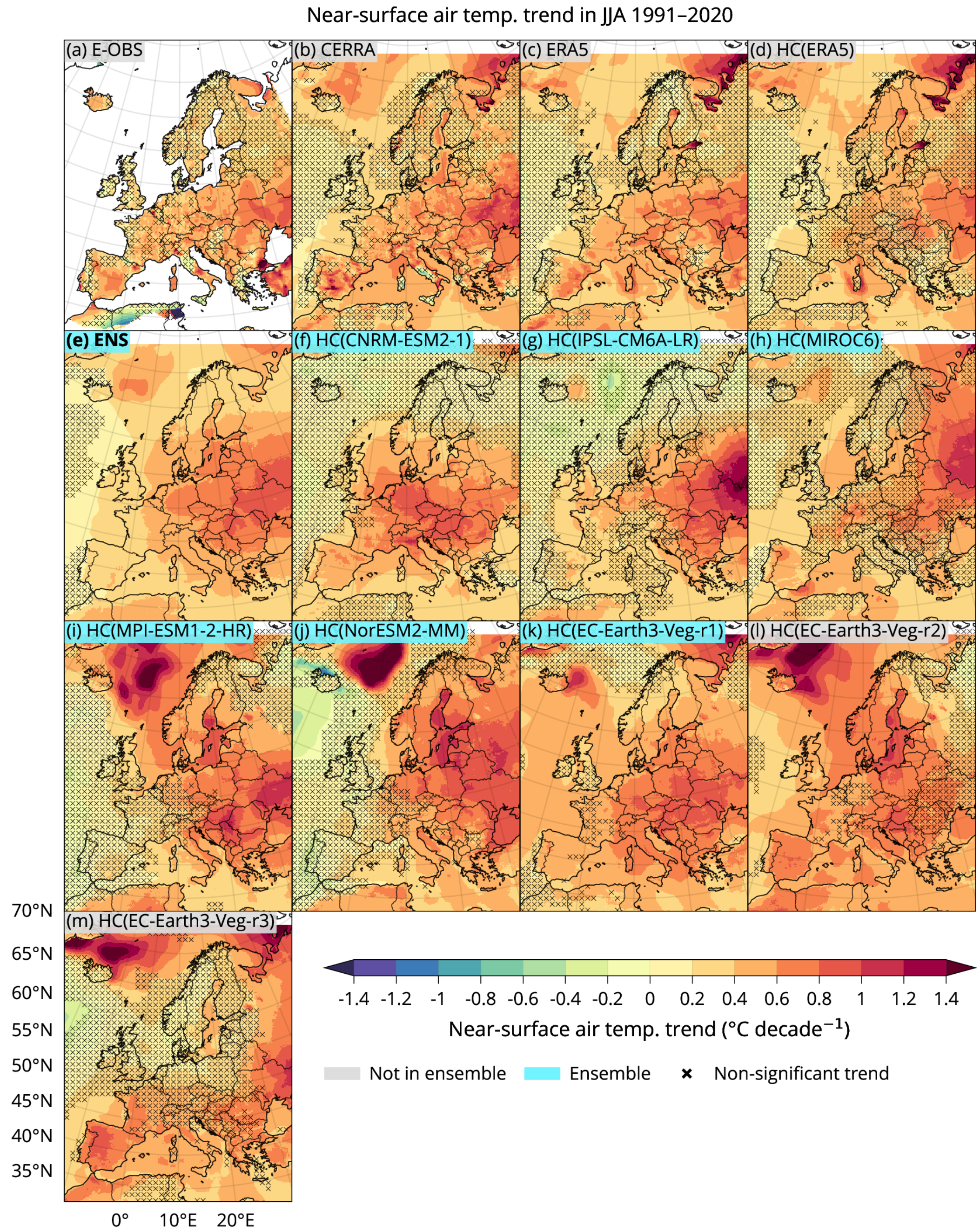

Figure 8. The same as Fig. 7 but for summer.

However, small-scale features can be different among the three datasets. For example, E-OBS shows localised patches of cooling in Southern Europe that are not apparent in CERRA or ERA5. A common feature across all three datasets is a weak cooling signal over northern Scandinavia. ERA5-driven simulation (Fig. 7d) underestimates the observed winter trends in the northeastern part of the domain, while overestimating them in parts of the southeast. The GCM-driven simulations (Fig. 7e–m) show various spatial patterns of the simulated trends. Simulations driven by MIROC6, MPI-ESM1-2-HR, IPSL-CM6A-LR, and EC-Earth3-Veg-r2 (Fig. 7h, i, g, and l) substantially overestimate the trends across large parts of the domain, whereas the simulations driven by CNRM-ESM2-1 and NorESM2-MM (Fig. 7f and j) underestimate the trends over the Iberian Peninsula but overestimate over Central Europe (CNRM-ESM2-1) and Eastern Europe and the Baltic (NorESM2-MM). The ensemble mean offsets the oppositely signed biases present in the individual GCM-driven simulations and reproduces a warming pattern that broadly resembles the observations, although some biases persist.

The three members of the EC-Earth3-Veg-driven ensemble (Fig. 7k–m) exhibit markedly different patterns of simulated winter temperature trends, with r3 reproducing the observed trend pattern more closely than r1 and r2. The three simulations differ only in their initial conditions, unlike the other HCLIM simulations, which differ in the boundary conditions set by the driving GCM. The effect of the initial conditions on the results highlights the dominant role of natural variability in shaping simulated wintertime regional temperature trends over Europe. This highlights the need for large ensembles to reproduce the observed trends in the ensemble mean. However, averaging across all simulations suppresses the contribution of natural variability, which itself accounts for part of the temperature trends. Therefore, the ensemble mean is not generally expected to perfectly reproduce wintertime temperature trends over Europe for time periods when natural variability plays a dominant role.

In summer, the observed temperature trends are significant across a substantial part of Europe, excluding the Atlantic and Northern Europe (Fig. 8a–c). However, the regional patterns of non-significant trends in Northern Europe differ among the datasets. E-OBS shows warming of about 0.6 °C per decade over Western and Central Europe, increasing up to 1 °C per decade in Eastern Europe. A similar spatial pattern is evident in both CERRA and ERA5, although with a tendency toward slightly higher trend values. E-OBS and CERRA show small non-significant patches of negative trends in Southern Europe, such as in the Apennine Peninsula, whereas ERA5 indicates positive temperature trends across the same regions. The ERA5-driven evaluation simulation (Fig. 8d) exhibits a broadly similar trend pattern on average, but the trends are non-significant over many regions where the observational datasets indicate significant temperature changes. In contrast, significant trends are evident across most of Scandinavia. The GCM-driven simulations (Fig. 8e–m) show varying trend patterns, although five of the six simulations included in the ensemble mean, with the exception of HCLIM(CNRM-ESM2-1) (Fig. 8f), reproduce spatial patterns that broadly resemble the observations. As a result, the ensemble mean reproduces the observed trend pattern reasonably well. The three members of the HCLIM ensemble driven by the three EC-Earth3-Veg members (Fig. 8k–m) show large regional differences in the simulated summer temperature trends. For example, the third member simulates near-zero trends over Northern Europe, in contrast to the first and second members. These differences indicate that, even in summer, natural variability plays an important role in shaping temperature trend patterns across Europe.

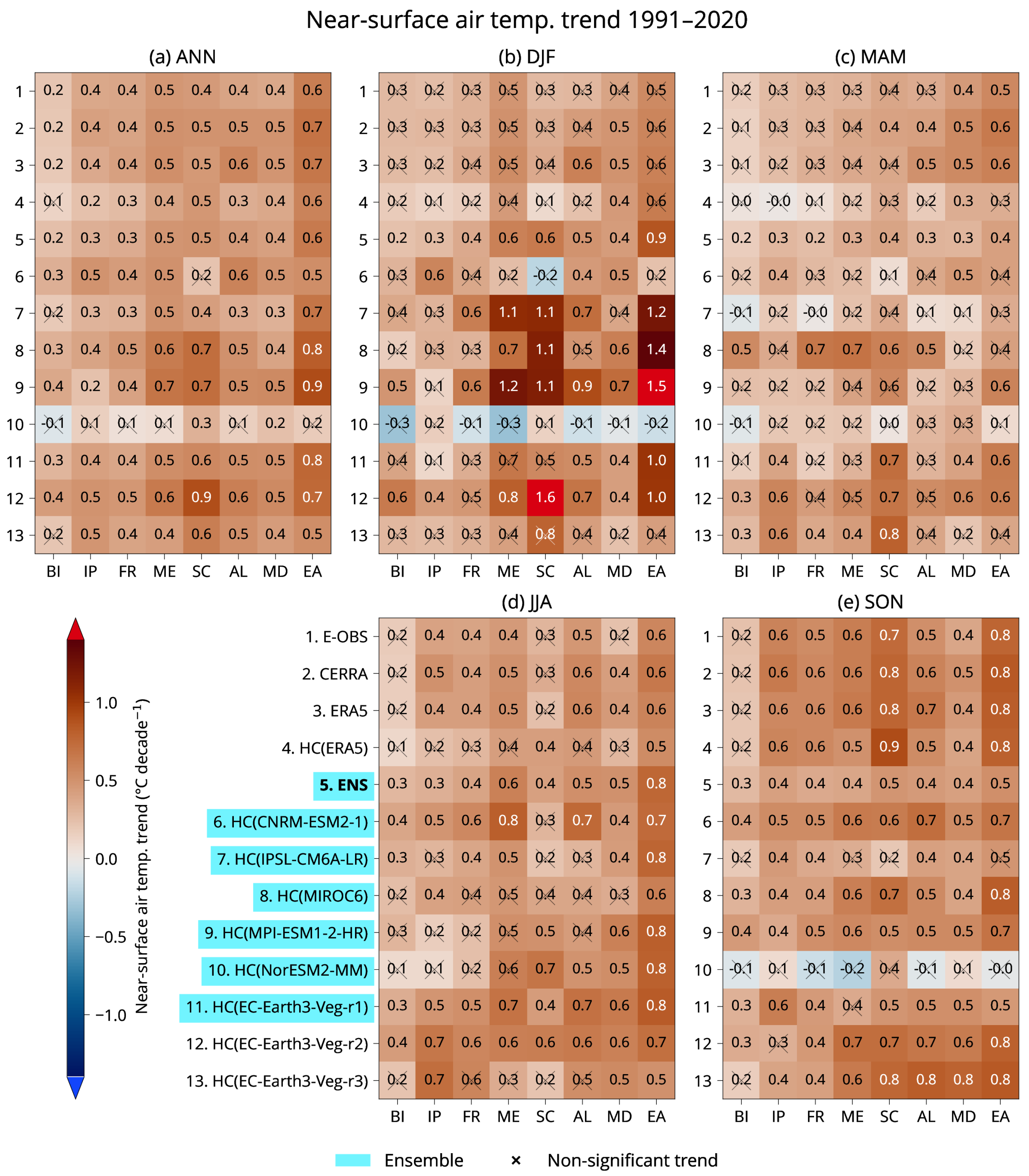

Figure 9. The same as Fig. 5 but for linear trends and all values shown as absolute values (i.e., not relative to E-OBS). Non-significant trends are marked with a cross.

3.3.2 Regional trends

Figure 9 summarises the observed and simulated near-surface air temperature trends, showing seasonal and annual mean trends across the PRUDENCE regions. All observational datasets consistently show a warming trend across Europe and exhibit strong agreement across all seasons and PRUDENCE regions. The discrepancies among the observations are minor, with average differences of approximately 0.1 °C per decade. Most HCLIM simulations also show a warming trend, although substantial differences in the magnitude of the trends are evident across seasons, regions, and simulations. For example, the simulations driven by IPSL-CM6A-LR, MPI-ESM1-2-HR, and MIROC6 substantially overestimate the observed winter temperature trends by a factor of 2–3 over Scandinavia, Eastern Europe, and the Mediterranean region. The EC-Earth3-Veg ensemble exhibits substantial spread in winter temperature trends among its individual members, over Scandinavia and Eastern Europe, again stressing the importance of natural variability. A notable feature is the underestimation of the observed warming trends and in some cases even cooling in the HCLIM run driven by NorESM2-MM, especially for winter, autumn, and annual mean temperatures.

3.4 Comparison of the global and downscaled models

In general, RCMs are expected to provide added value (understood as an improved representation of climatology) relative to the driving GCMs. This includes a better representation of regional and local weather and climate features as a result of higher resolution and enhanced ability to capture small-scale processes. However, like all climate models, RCMs provide only an approximation of the real climate system and are subject to various errors (biases) that lead to deviations between the simulated and observed climates. In addition to their higher resolution, differences between RCMs and their driving GCMs may also arise from differences in model formulation (e.g., physical schemes and parameterizations) as well as from differences in external forcing and its implementation (e.g., aerosols). These factors are expected to introduce deviations of the RCMs from the driving model or reanalysis, potentially resulting in simulations that differ more from the observational reference than the driving models themselves.

Figure 10 illustrates near-surface air temperature and precipitation anomalies from the E-OBS observations shown as arrows connecting the driving GCM/reanalysis to the corresponding HCLIM simulations. As shown in the previous results, E-OBS, CERRA, and ERA5 tend to cluster relatively close to one another compared to the GCMs and HCLIM simulations. This suggests that the reference datasets (E-OBS and the reanalyses) are generally consistent with each other, although their differences are still non-negligible relative to the magnitude of the model biases. Some of the largest differences between the driving GCMs and HCLIM simulations are found for MIROC6. This is particularly pronounced for temperature, where the differences are on the order of 1–3 °C, and, to a lesser extent, for precipitation, with the HCLIM(MIROC6) simulation generally moving closer to the observations, although not consistently in all cases. The exceptions occur in winter over Mid-Europe, Scandinavia, the Alps, and Eastern Europe (Fig. 10d, e, f, and h), where the HCLIM(MIROC6) simulation deviates further in temperature from the observational reference than MIROC6. In many subsets, smaller shifts are found for CNRM-ESM2-1 and NorESM2-MM in both temperature and precipitation. For CNRM-ESM2-1, these shifts are mixed, with some changes bringing the HCLIM simulation

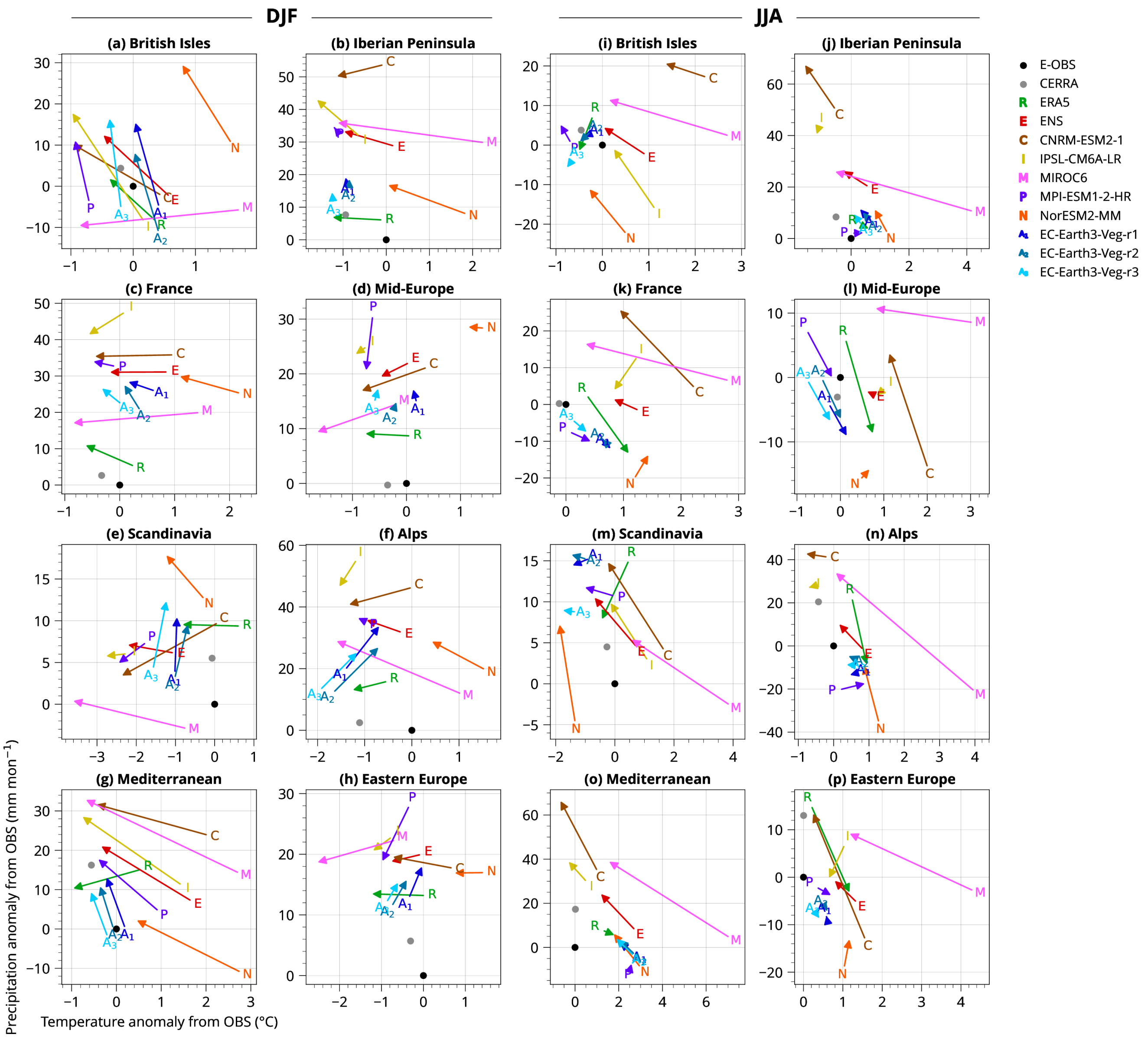

Figure 10. Scatter plots showing near-surface air temperature and precipitation anomalies from the E-OBS observations for the CERRA(-Land) and ERA5 reanalyses, the HCLIM ensemble (ENS), and the GCM-driven HCLIM simulations in each PRUDENCE region in **(a–h)** winter and **(i–p)** summer. The points are shown in pairs of the global model/reanalysis connected by an arrow pointing to the corresponding HCLIM simulation driven by the model/reanalysis. E-OBS and CERRA(-Land) are shown as individual points since they do not have a corresponding HCLIM simulation. CERRA is used for temperature and CERRA-Land for precipitation due to the limitations described in Section 2.2, both of which are labelled as 'CERRA'.

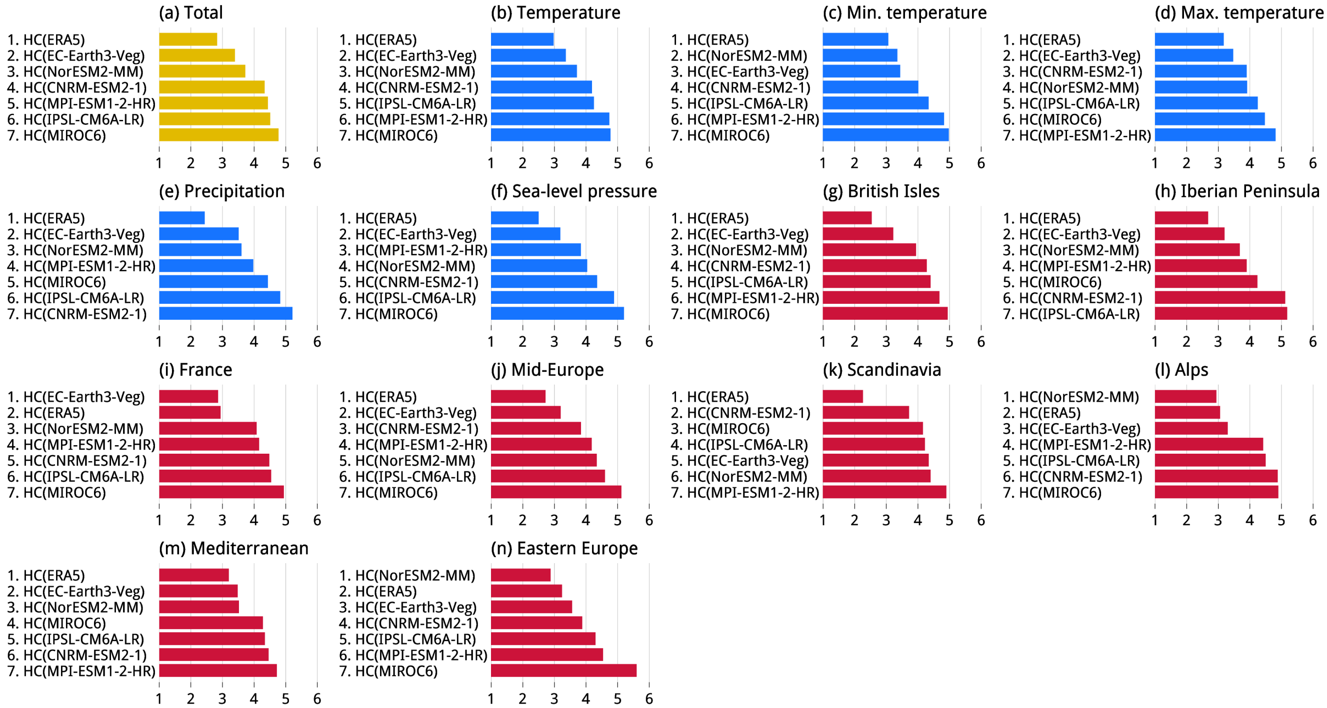

Figure 11. The HCLIM model ranks based on the E-OBS (all variables except SLP) and ERA5 (SLP) reference and time period 1991–2020. Shown is **(a)** the total rank [for all variables and all regions; Eq. (1)] and **(b–f)** ranks for individual variables [all regions; Eq. (2)]: mean, daily minimum (min.), and daily maximum (max.) near-surface air temperature, precipitation, and SLP, as well as **(g–n)** ranks for the PRUDENCE regions [all variables; Eq. (3)]. Only the run r1 of EC-Earth3-Veg is included in the results. The model ranking method is described in Section 3.5.

closer to the observations, others moving it further away, and some having little overall effect. For NorESM2-MM, these shifts generally move the HCLIM simulation closer to the observations, although exceptions occur in winter for the British Isles and Scandinavia, where the deviations increase relative to the observational reference. The smallest differences are found between HCLIM(EC-Earth3-Veg), and EC-Earth3-Veg. The shifts from ERA5 to HCLIM(ERA5) are relatively moderate compared to those found for other driving GCM–HCLIM pairs and, in many cases, move the HCLIM simulation further away from the observations. The HCLIM simulations, relative to the driving simulation, tend to decrease near-surface air temperature and its bias relative to observations and increase precipitation and its bias.

3.5 Model ranking

Ranking climate simulations according to their ability to reproduce various aspects of the observed climate is a common approach for identifying the best-performing simulations. However, such rankings are inherently subjective, as they depend on the choice and number of metrics included in the analysis. Figure 11 shows the ranking of the HCLIM simulations based on the mean and standard deviation of the five most commonly analysed variables: mean, daily minimum and maximum near-surface air temperature, precipitation, and SLP. The lowest rank signifies the best-performing simulation, and the highest rank the worst-performing. As expected, the evaluation simulation driven by the reanalysis ERA5 performs best in the overall ranking (Fig. 11a). Among the GCM-driven simulations, HCLIM(EC-Earth3-Veg) achieves the best overall rank, followed by HCLIM(NorESM2-MM), whereas HCLIM(MIROC6) is the worst-performing simulation. The performance for the individual variables (Fig. 11b–f) generally mirrors the overall ranking, although with some notable differences. HCLIM(NorESM2-MM) is the best-performing GCM-driven simulation for daily minimum temperature (Fig. 11c), while the highest ranks are held by HCLIM(MPI-ESM1-2-HR) and HCLIM(CNRM-ESM2-1) in daily maximum temperature (Fig. 11d) and precipitation (Fig. 11e), respectively. When ranking by region (Fig. 11g–n), HCLIM(ERA5) is not always the best-performing simulation: HCLIM(EC-Earth3-Veg) is the best simulation in France and the Alps (Fig. 11i and l) and HCLIM(NorESM2-MM) in Eastern Europe (Fig. 11n). While HCLIM(MIROC6) is the worst-performing simulation in most regions, the highest rank is instead held by HCLIM(IPSL-CM6A-LR) over the Iberian Peninsula (Fig. 11h) and by HCLIM(MPI-ESM1-2-HR) over Scandinavia and the Mediterranean (Fig. 11k and m). Scandinavia (Fig. 11k) stands out from the other regions in that HCLIM(EC-Earth3-Veg) performs comparatively poorly there, whereas HCLIM(MIROC6) performs relatively well, and the best-performing GCM-driven simulation is HCLIM(CNRM-ESM2-1).

4 Discussion

A detailed investigation of the causes of the HCLIM biases is beyond the scope of the present study, which focuses primarily on providing a reference description of the HCLIM ensemble. However, biases in the large-scale circulation of the driving GCMs are discussed here, along with their potential influence on temperature and precipitation biases in the HCLIM simulations. GCM-driven RCM simulations typically exhibit larger biases than reanalysis-driven simulations, as they combine intrinsic structural deficiencies of RCMs with biases inherited from the driving GCMs. Nevertheless, these two error sources may partially offset one another in some cases, leading to a reduced overall bias despite the presence of substantial underlying model errors. Large-scale atmospheric circulation is one of the dominant drivers of European climate variability, strongly influencing temperature, precipitation, wind, and extreme events, especially during winter (Hurrell et al., 2003). Consequently, substantial biases in the representation of large-scale circulation by the driving GCMs propagate to RCM simulations, leading to pronounced deviations from observations in the downscaled climate fields (van Ulden et al., 2007; Kjellström et al., 2011).

In winter, MIROC6 shows a pronounced SLP bias, characterised by an underestimation of the climatological high-pressure area south of Scandinavia and an overestimation of the Arctic low (Fig. S2g). This dipolar bias pattern weakens the meridional pressure gradient, resulting in an under-representation of the prevailing westerly circulation over Europe. The same dipolar SLP bias pattern is clearly evident in the HCLIM simulation driven by MIROC6 (Fig. S3h), which receives the poorest ranking for the simulated SLP among all simulations (Fig. 11f). The weakened zonal circulation in MIROC6 and HCLIM(MIROC6) favours a more meridional flow regime, increasing the frequency of cold-air intrusions from the Arctic. This circulation bias likely contributes to the pronounced cold bias in HCLIM(MIROC6) over the eastern part of the domain, as evident in Fig. 1h.

Wintertime SLP biases associated with a weakened zonal circulation are also evident, to varying degrees, in IPSL-CM6A-LR, CNRM-ESM2-1, and MPI-ESM1-2-HR (Fig. S2f, e, and h). These large-scale circulation biases are propagated into the corresponding HCLIM simulations (Fig. S3g, f, and i), which generally simulate a colder climate in the northern part of the domain (Fig. 1g, f, and i) than the ERA5-driven simulation.

NorESM2-MM exhibits moderate SLP biases that favour a stronger zonal flow regime, and these SLP biases are also clearly reproduced in the corresponding HCLIM simulation. A stronger zonal flow regime in HCLIM(NorESM2-MM) likely contributes to the warm bias over Western and Central Europe (Fig. 1), whereas the corresponding ERA5-driven simulation exhibits a cold bias. The three HCLIM simulations driven by the EC-Earth3-Veg ensemble show the smallest wintertime temperature biases (Fig. 1k–m), consistent with the comparatively small SLP biases in the driving GCM (Fig. S2j–l). This highlights the critical role of accurately simulating large-scale atmospheric circulation in the driving GCM for reproducing near-surface temperatures in the downscaled simulations. In summer, the largest SLP biases occur in MIROC6, which strongly underestimates SLP in the southern part of the domain, and in CNRM-ESM2-1, which overestimates SLP over the northwestern part of the domain (Fig. S4g and e). The other GCMs display minor (EC-Earth3-Veg and MPI-ESM1-2-HR) to moderate (IPSL-CM6A-LR and NorESM2-MM) biases. HCLIM largely retains these spatial bias patterns but generally attenuates their magnitude (Fig. S5).

Attribution of summer temperature biases in the HCLIM simulations to SLP biases in the driving GCMs is not straightforward. Across all GCM-driven simulations, HCLIM reproduces the large-scale temperature bias pattern similar to one found in the ERA5-driven experiment, indicating a dominant contribution from structural model biases (Fig. 2d–m). The pattern consists of a cold bias in the northern part of the domain and a warm bias in the southern part. However, the magnitude of the biases present in HCLIM(ERA5) (Fig. 2d) can be amplified, as demonstrated by HCLIM(NorESM2-MM) (Fig. 2j), which shows a stronger cold bias in the northern part of the domain. In contrast, the sign of the bias may even reverse, as in the CNRM-ESM2-1- and IPSL-CM6A-LR-driven simulations over Southern Europe (Fig. 2f–g). This cold bias coincides with the exceptionally large wet biases in these simulations (Fig. 4f–g and 6d), suggesting a possible link between excessive precipitation and cooler near-surface temperatures; this link, however, is not present in the other GCM-driven simulations.

Precipitation is subject to larger observational uncertainties than temperature. Compared with E-OBS, CERRA-Land indicates wetter conditions over the eastern part of the domain, while ERA5 exhibits a widespread wet bias across most of the domain (Fig. 3c and 4c). The ERA5-driven HCLIM simulation largely reproduces the precipitation bias pattern present in ERA5 (Fig. 3c–d and 4c–d). In winter, all HCLIM simulations reproduce a broadly similar precipitation bias pattern south of Scandinavia, while the biases over Scandinavia are generally reduced (Fig. 3e–m). The NorESM2-MM-driven simulation exhibits an amplified wet bias extending from Western to Eastern Europe (Fig. 3j), consistent with a stronger zonal flow regime in NorESM2-MM that enhances the transport of Atlantic moisture into the continent (Fig. S4i).

Similar to winter, CERRA-Land indicates wetter conditions in Eastern Europe during summer (Fig. 4b), while ERA5 exhibits a widespread wet bias across much of the domain (Fig. 4c). When driven by ERA5, HCLIM produces a distinct dipole precipitation bias pattern, characterised by a wet bias over northern Scandinavia and a dry bias across Western and Southern Europe (Fig. 4d). This pattern is accompanied by localised regions of wet bias in southeastern parts of Europe and over the

Iberian Peninsula. This bias pattern is reproduced to some extent in the simulations driven by NorESM2-MM, MPI-ESM1-2-HR, and EC-Earth3-Veg (Fig. 4j, i, and k–m). In contrast, the CNRM-ESM2-1-, IPSL-CM6A-LR-, and MIROC6-driven simulations exhibit predominantly wet biases across the domain, with particularly large wet biases over the Mediterranean region (Fig. 4f–h).

The comparison between RCM and GCM simulations shows that a substantial improvement in the temperature bias relative to E-OBS is present in about 30% of GCM-driven RCM simulations (when summarised by season and region; Fig. 10) and worsening in about 25%. For precipitation, the opposite was true, with about 40% of RCM simulations worsening and 20% improving the bias compared to the driving GCM. For the EC-Earth3-Veg simulations, there was very little difference between the corresponding RCM and GCM simulations, possibly because of the similarity between the parameterisations employed by HCLIM43-ALADIN and EC-Earth3-Veg.

5 Conclusions

We analysed 30 years of data from six downscaled CMIP6 GCMs by the HCLIM43-ALADIN regional climate model over Europe and contrasted the results with the E-OBS gridded observations and three reanalyses (ERA5, CERRA, and CERRA-Land), focusing on near-surface air temperature and precipitation evaluation and employing sea-level pressure for the identification of circulation patterns potentially responsible for the biases. We used seasons and the PRUDENCE regions for spatiotemporal partitioning of the results. We also analysed temperature trends; how the RCM results compare with the driving GCMs; and compiled a model ranking based on a subjective choice of measures.

We find that the reanalyses are in overall good agreement with E-OBS, except for a small warm bias in ERA5 and a small negative bias in CERRA (within 1 °C). There is also larger cold bias in the evaluation run HCLIM(ERA5) in winter, but generally smaller than or comparable with the GCM-driven simulations. In winter, GCM-driven simulations have a substantial cold bias, especially over northeastern Europe (Fig. 1e–m), and positive biases in summer in Central and Southern Europe (Fig. 2e–m). Cold bias is prevalent across almost all GCM-driven simulations and regions in spring (Fig. 5c). In general, in the GCM-driven simulations, cold biases are present in the northeast and warm biases in the south, both in winter and summer. The HCLIM(ERA5) simulation exhibits substantially different temperature biases from the driving ERA5 reanalysis (Fig. 1c–d, 2c–d, and 5), but the temperature trends appear very similar (Fig. 7c–d, 8c–d, and 9). This indicates that the RCM imprints its own biases, but the trends are to a large extent determined by the driving data. A wet bias relative to E-OBS is present in the reanalyses and more so in the HCLIM simulations, especially in winter and spring, and less so in summer and autumn (Fig. 6d and e). In summer, a wet bias in the GCM-driven simulations is very pronounced in Southern Europe (the Iberian Peninsula and Mediterranean), where this is also amplified by the low precipitation totals (Fig. 4e–m).

The three EC-Earth3-Veg simulations with different initial conditions show very similar biases, indicating that internal variability is small relative to the overall biases, but there are notable differences in parts of our analysis. The r3 simulation is colder and wetter than r1 and r2 (Fig. 5 and 6). In winter, the near-surface air temperature trend is also much more positive in r2 than in r1 and r3, and more neutral in r3 than in the other two simulations in both winter and summer (Fig. 7k–m, 8k–m, and 9b and d).

Some SLP biases can be identified as a source of temperature and precipitation biases through their effect on large-scale circulation, affecting, for example, the prevailing westerly circulation in Europe (Fig. S2–5). Especially, this is the case in MIROC6 and the MIROC6-driven simulation, but to a lesser extent in the other GCM-driven simulations, where weakened zonal circulation might promote cold air intrusions from the Arctic in winter, resulting in cold bias in northeastern Europe. Biases in quantities other than SLP, such as clouds, might also contribute to the near-surface air temperature and precipitation biases.

Over the 30-year period, a significant warming trend of about 0.5 °C per decade, and regionally and seasonally up to 1.5 °C per decade, is present in the observations, reanalyses, and simulations over large areas of continental Europe in summer, but in winter the trends are significant only in some simulations over Central, Eastern, and northeastern Europe (Fig. 7 and 8). In summer, the trends are mostly significant over all land areas. The period is probably too short to reliably detect winter trends given the natural variability. When averaged by regions, however, the trends are significant in the majority of cases in summer and autumn and about half of the cases in winter and spring (Fig. 9).

Compared with the driving GCMs, RCMs can be affected both by biases in the driving GCM, biases in the RCM, their constructive or destructive interference, as well as mismatches between the model formulation and the forcings (Fig. 10). We see close clustering of the observations and reanalyses but greater differences between the corresponding GCM and RCM simulations, especially for MICROC6. Very small GCM–RCM differences are for the EC-Earth3-Veg simulations, possibly due to the commonalities between EC-Earth and ALADIN. While in many cases we see an improved representation of temperature and precipitation in the RCM simulations over the driving GCM, the opposite is not uncommon, and, in fact, is more prevalent for precipitation. This means that HCLIM does not always improve large-scale biases relative to the driving GCM and can make them worse.

We constructed model ranking based on biases in a number of common physical quantities and the PRUDENCE regions compared with E-OBS and ERA5 (Fig. 11), while recognising that this is a subjective choice and past model performance does not necessarily determine future performance or correct representation of weather and climate processes. Unsurprisingly, the evaluation (ERA5-driven) simulation performed the best. Across the quantities and regions, HCLIM(EC-Earth3-Veg) and HCLIM(NorESM2-MM) tended to be the best-performing GCM-driven simulations, and HCLIM(MIROC6) the worst-performing simulation, probably because of its misrepresentation of SLP over Europe. Scandinavia, however, was an exception in terms of the ranking, with HCLIM(CNRM-ESM2-1) performing best and HCLIM(MIROC6) performing relatively well.

Future projections for the 21st century by HCLIM43-ALADIN for the same set of downscaled GCMs will be analysed in a separate publication. Analyses of the past and future scenario simulations by the entire multi-RCM-multi-GCM EURO-CORDEX-CMIP6 ensemble are in preparation by the project members. Because we have not attempted to further investigate the physical reasons for the biases due to a limited scope, further studies would be needed to fill this gap. The model output data of the EURO-CORDEX-CMIP6 ensemble will be made available publicly on the Earth System Grid Federation (ESGF; ESGF, 2026a), ready for use for further analyses by the scientific community and decision-making.

Code and data availability. The data processing and plotting code used in our analysis is publicly available on GitHub (Kuma, 2026a) and Zenodo (Kuma, 2026b). The HARMONIE-Climate (HCLIMcom, 2006) model is jointly developed by its 9 member institutes. HCLIM is part of the ACCORD consortium (ACCORD, 2006). Access to the HCLIM source code for non-commercial research can be obtained by contacting a member institute in your home country, subject to a licence agreement specified by the ACCORD consortium. Some components of the HCLIM system can also be obtained by non-members through other licences, such as for OpenIFS (ECMWF, 2026b) for dynamics and Open-SURFEX (CNRM, 2026) for land surface processes. Full code access is provided to the journal editor and reviewers through a research licence. The downscaled HCLIM model data are currently being uploaded and will be publicly available from the ESGF MetaGrid (ESGF, 2026b) and CORDEX (CORDEX, 2026). The CMIP6 global model data are publicly available from the ESGF MetaGrid (ESGF, 2026b). The E-OBS gridded observation data (UERRA et al., 2026), the CERRA reanalysis (Schimanke et al., 2021), the CERRA-Land reanalysis (Verrelle et al., 2022) and the ERA5 reanalysis (Hersbach et al., 2017) are publicly available from the Copernicus Climate Change Service (C3S).

Author contributions. Conceptualization: GN and PK; data curation: GN, PK, AAC, AD, JL, MS, FB, and CN; formal analysis: GN and PK; funding acquisition: GN; investigation: GN, PK, FW, BvU, AD, JCS, MS, OBC, FB, PS, and CN; methodology: GN, PK, and BvU; project administration: GN, OL, and AD; software: GN, PK, BvU, JCS, JL, MS, OBC, PS, and CN; supervision: GN; visualization: GN and PK; writing (original draft preparation): GN and PK; and writing (review and editing): all authors.

Competing interests. The authors declare that they have no conflict of interest.

Acknowledgements. This study has been made possible thanks to support from the Rossby Centre at SMHI, which provided the downscaled climate simulation data together with DMI and MET Norway as a contribution to the international CORDEX project. The simulations used global simulations from the CMIP6, available through the ESGF nodes, including the Swedish node funded by SMHI and operated by the National Supercomputer Centre (NSC). The regional computations and data handling were enabled by resources provided by SMHI, operated by the NSC, the climate modelling infrastructure and staff at the Rossby Centre and SMHI, as well as computing and storage facilities from the ECMWF. We acknowledge funding from the Bolin Centre. We acknowledge the E-OBS dataset from the EU-FP6 project UERRA (UERRA, 2026) and C3S, and the data providers in the ECA&D project (ECA&D, 2026); the CERRA and CERRA-Land reanalyses provided by SMHI, MET Norway, and Météo-France and hosted by C3S; and the ERA5 reanalysis provided by the ECMWF and hosted by C3S. We acknowledge the WCRP's Working Group on Coupled Modelling, which is responsible for CMIP, and we thank the climate modeling groups (listed in Table 1) for producing and making available their model output. For CMIP the U.S. Department of Energy's Program for Climate Model Diagnosis and Intercomparison provides coordinating support and led development of software infrastructure in partnership with the Global Organization for Earth System Science Portals. Last but not least, our analysis was made possible thanks to the open-source software Python (Van Rossum, 2003), NumPy (Harris et al., 2020), Matplotlib (Hunter, 2007), CDO (Schulzweida, 2023), parallel (Tange, 2011), cartopy (Met Office, 2010), SciPy (Virtanen et al., 2020), Bash (Fox et al., 2025), pyproj (Whitaker and contributors, 2026), NetCDF (Rew and Davis, 1990), HDF (Folk et al., 1999), and GNU/Linux (Stallman, 1985; Torvalds, 1997).

References

ACCORD: ACCORD: A Consortium for COnvection-scale modelling Research and Development, https://www.umr-cnrm.fr/accord/, last access: 2 September 2026, 2006.

Ban, N., Caillaud, C., Coppola, E., Pichelli, E., Sobolowski, S., Adinolfi, M., Ahrens, B., Alias, A., Anders, I., Bastin, S., Belušić, D., Berthou, S., Brisson, E., Cardoso, R. M., Chan, S. C., Christensen, O. B., Fernández, J., Fita, L., Frisius, T., Gašparac, G., Giorgi, F., Goergen, K., Haugen, J. E., Hodnebrog, O., Kartsios, S., Katragkou, E., Kendon, E. J., Keuler, K., Lavín-Gullón, A., Lenderink, G., Leutwyler, D., Lorenz, T., Maraun, D., Mercogliano, P., Milovac, J., Panitz, H.-J., Raffa, M., Reca Remedio, A., Schär, C., Soares, P. M. M., Srnec, L., Steensen, B. M., Stocchi, P., Tölle, M. H., Truhetz, H., Vergara-Temprado, J., de Vries, H., Warrach-Sagi, K., Wulfmeyer, V., and Zander, M. J.: The first multi-model ensemble of regional climate simulations at kilometer-scale resolution, part I: evaluation of precipitation, Climate Dynamics, 57, 275–302, https://doi.org/10.1007/s00382-021-05708-w, 2021.

Batrak, Y., Kourzeneva, E., and Homleid, M.: Implementation of a simple thermodynamic sea ice scheme, SICE version 1.0-38h1, within the ALADIN–HIRLAM numerical weather prediction system version 38h1, Geoscientific Model Development, 11, 3347–3368, https://doi.org/10.5194/gmd-11-3347-2018, 2018.

Belušić, D., de Vries, H., Dobler, A., Landgren, O., Lind, P., Lindstedt, D., Pedersen, R. A., Sánchez-Perrino, J. C., Toivonen, E., van Ulft, B., Wang, F., Andrae, U., Batrak, Y., Kjellström, E., Lenderink, G., Nikulin, G., Pietikäinen, J.-P., Rodríguez-Camino, E., Samuelsson, P., van Meijgaard, E., and Wu, M.: HCLIM38: a flexible regional climate model applicable for different climate zones from coarse to convection-permitting scales, Geoscientific Model Development, 13, 1311–1333, https://doi.org/10.5194/gmd-13-1311-2020, 2020.

Berthou, S., J Roberts, M., Vannière, B., Ban, N., Belušić, D., Caillaud, C., Crocker, T., de Vries, H., Dobler, A., Harris, D., J Kendon, E., Landgren, O., and Manning, C.: Convection in future winter storms over Northern Europe, Environmental Research Letters, 17, 114 055, https://doi.org/10.1088/1748-9326/aca03a, 2022.

Boone, A.: Description du schéma de neige ISBA-ES (Explicit Snow), Note de Centre No. 70, Centre National de Recherches Météorologiques and Météo-France, Toulouse, France, https://www.umr-cnrm.fr/surfex/IMG/pdf/10_snowdoc.pdf, 2002.

Boucher, O., Servonnat, J., Albright, A. L., Aumont, O., Balkanski, Y., Bastrikov, V., Bekki, S., Bonnet, R., Bony, S., Bopp, L., Braconnot, P., Brockmann, P., Cadule, P., Caubel, A., Cheruy, F., Codron, F., Cozic, A., Cugnet, D., D'Andrea, F., Davini, P., de Lavergne, C., Denvil, S., Deshayes, J., Devilliers, M., Ducharne, A., Dufresne, J.-L., Dupont, E., Éthé, C., Fairhead, L., Falletti, L., Flavoni, S., Foujols, M.-A., Gardoll, S., Gastineau, G., Ghattas, J., Grandpeix, J.-Y., Guenet, B., Guez, Lionel, E., Guilyardi, E., Guimberteau, M., Hauglustaine, D., Hourdin, F., Idelkadi, A., Joussaume, S., Kageyama, M., Khodri, M., Krinner, G., Lebas, N., Levavasseur, G., Lévy, C., Li, L., Lott, F., Lurton, T., Luyssaert, S., Madec, G., Madeleine, J.-B., Maignan, F., Marchand, M., Marti, O., Mellul, L., Meurdesoif, Y., Mignot, J., Musat, I., Ottlé, C., Peylin, P., Planton, Y., Polcher, J., Rio, C., Rochetin, N., Rousset, C., Sepulchre, P., Sima, A., Swingedouw, D., Thiéblemont, R., Traore, A. K., Vancoppenolle, M., Vial, J., Vialard, J., Viovy, N., and Vuichard, N.: Presentation and Evaluation of the IPSL-CM6A-LR Climate Model, Journal of Advances in Modeling Earth Systems, 12, e2019MS002 010, https://doi.org/10.1029/2019MS002010, 2020.

Bougeault, P.: A Simple Parameterization of the Large-Scale Effects of Cumulus Convection, Monthly Weather Review, 113, 2108–2121, https://doi.org/10.1175/1520-0493(1985)113<2108:ASPOTL>2.0.CO;2, 1985.

Bougeault, P. and Lacarrere, P.: Parameterization of Orography-Induced Turbulence in a Mesobeta–Scale Model, Monthly Weather Review, 117, 1872–1890, https://doi.org/10.1175/1520-0493(1989)117<1872:POOITI>2.0.CO;2, 1989.

Bouteloup, Y., Bouyssel, F., and Marquet, P.: Improvements of Lopez's prognostic large-scale cloud and precipitation scheme, ALADIN Newsletter 28, https://www.cnrm.meteo.fr/aladin/IMG/pdf/N28_PAPER.pdf, last access: 3 September 2026, 2005.

Boé, J., Somot, S., Corre, L., and Nabat, P.: Large discrepancies in summer climate change over Europe as projected by global and regional climate models: causes and consequences, Climate Dynamics, 54, 2981–3002, https://doi.org/10.1007/s00382-020-05153-1, 2020.

Buizza, R., Alonso, M., Balmaseda, M. A., Brown, A., English, S. J., Forbes, R., Geer, A. J., Haiden, T., Leutbecher, M., Magnusson, L., Rodwell, M., Sleigh, T., Stockdale, T., Vitart, F., and Wedi, N.: The development and evaluation process followed at ECMWF to upgrade the Integrated Forecasting System (IFS), ECMWF Technical Memoranda No. 829, European Centre for Medium-Range Weather Forecasts (ECMWF), Reading, UK, https://doi.org/10.21957/xzopnhty9, 2018.

Christensen, J. H. and Christensen, O. B.: A summary of the PRUDENCE model projections of changes in European climate by the end of this century, Climatic Change, 81, 7–30, https://doi.org/10.1007/s10584-006-9210-7, 2007.

Christensen, J. H., Carter, T. R., Rummukainen, M., and Amanatidis, G.: Evaluating the performance and utility of regional climate models: the PRUDENCE project, Climatic Change, 81, 1–6, https://doi.org/10.1007/s10584-006-9211-6, 2007a.

Christensen, O. B., Drews, M., Hesselbjerg Christensen, J., Dethloff, K., Ketelsen, K., Hebestadt, I., and Rinke, A.: The HIRHAM Regional Climate Model. Version 5 (beta), Report 06-17, Danish Climate Centre and Danish Meteorological Institute, Copenhagen, Denmark, https://backend.orbit.dtu.dk/ws/portalfiles/portal/51950450/HIRHAM.pdf, 2007b.

CNRM: SURFEX: Surface modelling platform, https://www.umr-cnrm.fr/surfex/, last access: 2 September 2026, 2026.

Copernicus Climate Change Service (C3S): Copernicus Interactive Climate Atlas, https://atlas.climate.copernicus.eu/atlas, last access: 28 August 2026, 2026.

Coppola, E., Sobolowski, S., Pichelli, E., Raffaele, F., Ahrens, B., Anders, I., Ban, N., Bastin, S., Belda, M., Belušić, D., Caldas-Alvarez, A., Cardoso, R. M., Davolio, S., Dobler, A., Fernandez, J., Fita, L., Fumière, Q., Giorgi, F., Goergen, K., Güttler, I., Halenka, T., Heinzeller, D., Hodnebrog, Ø., Jacob, D., Kartsios, S., Katragkou, E., Kendon, E., Khodayar, S., Kunstmann, H., Knist, S., Lavín-Gullón, A., Lind, P., Lorenz, T., Maraun, D., Marelle, L., van Meijgaard, E., Milovac, J., Myhre, G., Panitz, H.-J., Piazza, M., Raffa, M., Raub, T., Rockel, B., Schär, C., Sieck, K., Soares, P. M. M., Somot, S., Srnec, L., Stocchi, P., Tölle, M. H., Truhetz, H., Vautard, R., de Vries, H., and Warrach-Sagi, K.: A first-of-its-kind multi-model convection permitting ensemble for investigating convective phenomena over Europe and the Mediterranean, Climate Dynamics, 55, 3–34, https://doi.org/10.1007/s00382-018-4521-8, 2020.

Coppola, E., Nogherotto, R., Ciarlo', J. M., Giorgi, F., van Meijgaard, E., Kadygrov, N., Iles, C., Corre, L., Sandstad, M., Somot, S., Nabat, P., Vautard, R., Levavasseur, G., Schwingshackl, C., Sillmann, J., Kjellström, E., Nikulin, G., Aalbers, E., Lenderink, G., Christensen, O. B., Boberg, F., Sørland, S. L., Demory, M.-E., Bülow, K., Teichmann, C., Warrach-Sagi, K., and Wulfmeyer, V.: Assessment of the European Climate Projections as Simulated by the Large EURO-CORDEX Regional and Global Climate Model Ensemble, Journal of Geophysical Research: Atmospheres, 126, e2019JD032 356, https://doi.org/10.1029/2019JD032356, 2021.

CORDEX: Coordinated Regional Climate Downscaling Experiment: Data access, https://cordex.org/data-access/, last access: 14 September 2026, 2026.

Cornes, R. C., van der Schrier, G., van den Besselaar, E. J. M., and Jones, P. D.: An Ensemble Version of the E-OBS Temperature and Precipitation Data Sets, Journal of Geophysical Research: Atmospheres, 123, 9391–9409, https://doi.org/10.1029/2017JD028200, 2018.

Cuxart, J., Bougeault, P., and Redelsperger, J.-L.: A turbulence scheme allowing for mesoscale and large-eddy simulations, Quarterly Journal of the Royal Meteorological Society, 126, 1–30, https://doi.org/10.1002/qj.49712656202, 2000.

Danielson, J. and Gesch, D.: Global multi-resolution terrain elevation data 2010 (GMTED2010), Open-File Report No. 2011-1073, U.S. Geological Survey and Earth Resources Observation and Science (EROS) Center, https://doi.org/10.3133/ofr20111073, 2011.

Diez-Sierra, J., Iturbide, M., Gutiérrez, J. M., Fernández, J., Milovac, J., Cofiño, A. S., Cimadevilla, E., Nikulin, G., Levavasseur, G., Kjellström, E., Bülow, K., Horányi, A., Brookshaw, A., García-Díez, M., Pérez, A., Baño-Medina, J., Ahrens, B., Alias, A., Ashfaq, M., Bukovsky, M., Buonomo, E., Caluwaerts, S., Chou, S. C., Christensen, O. B., Ciarlò, J. M., Coppola, E., Corre, L., Demory, M.-E., Djurdjevic, V., Evans, J. P., Fealy, R., Feldmann, H., Jacob, D., Jayanarayanan, S., Katzfey, J., Keuler, K., Kittel, C., Kurnaz, M. L., Laprise, R., Lionello, P., McGinnis, S., Mercogliano, P., Nabat, P., Önol, B., Ozturk, T., Panitz, H.-J., Paquin, D., Pieczka, I., Raffaele, F., Remedio, A. R., Scinocca, J., Sevault, F., Somot, S., Steger, C., Tangang, F., Teichmann, C., Termonia, P., Thatcher, M., Torma, C., van Meijgaard, E., Vautard, R., Warrach-Sagi, K., Winger, K., and Zittis, G.: The Worldwide C3S CORDEX Grand Ensemble: A Major Contribution to Assess Regional Climate Change in the IPCC AR6 Atlas, Bulletin of the American Meteorological Society, 103, E2804–E2826, https://doi.org/10.1175/BAMS-D-22-0111.1, 2022.

Döscher, R., Acosta, M., Alessandri, A., Anthoni, P., Arsouze, T., Bergman, T., Bernardello, R., Boussetta, S., Caron, L.-P., Carver, G., Castrillo, M., Catalano, F., Cvijanovic, I., Davini, P., Dekker, E., Doblas-Reyes, F. J., Docquier, D., Echevarria, P., Fladrich, U., Fuentes-Franco, R., Gröger, M., v. Hardenberg, J., Hieronymus, J., Karami, M. P., Keskinen, J.-P., Koenigk, T., Makkonen, R., Massonnet, F., Ménégoz, M., Miller, P. A., Moreno-Chamarro, E., Nieradzik, L., van Noije, T., Nolan, P., O'Donnell, D., Ollinaho, P., van den Oord, G., Ortega, P., Prims, O. T., Ramos, A., Reerink, T., Rousset, C., Ruprich-Robert, Y., Le Sager, P., Schmith, T., Schrödner, R., Serva, F., Sicardi, V., Sloth Madsen, M., Smith, B., Tian, T., Tourigny, E., Uotila, P., Vancoppenolle, M., Wang, S., Wårlind, D., Willén, U., Wyser, K., Yang, S., Yepes-Arbós, X., and Zhang, Q.: The EC-Earth3 Earth system model for the Coupled Model Intercomparison Project 6, Geoscientific Model Development, 15, 2973–3020, https://doi.org/10.5194/gmd-15-2973-2022, 2022.

Druel, A., Munier, S., Mucia, A., Albergel, C., and Calvet, J.-C.: Implementation of a new crop phenology and irrigation scheme in the ISBA land surface model using SURFEX_v8.1, Geoscientific Model Development, 15, 8453–8471, https://doi.org/10.5194/gmd-15-8453-2022, 2022.

ECA&D: European Climate Assessment & Dataset, https://www.ecad.eu, last access: 9 September 2026, 2026.

ECMWF: IFS Documentation CY41R2 - Part IV: Physical Processes, IFS Documentation No. 4, European Centre for Medium-Range Weather Forecasts, Reading, UK, https://doi.org/10.21957/tr5rv27xu, 2016.

ECMWF: ECMWF Radiation Scheme Home, https://confluence.ecmwf.int/display/ECRAD, last access: 16 January 2026, 2026a.

ECMWF: ECMWF OpenIFS, GitHub [code], https://github.com/ecmwf-ifs/openifs, last access: 2 September 2026, 2026b.

ESCWA: Arab Climate Change Assessment Report – Main Report, Report E/ESCWA/SDPD/2017/RICCAR/Report, United Nations Economic and Social Commission for Western Asia, Beirut, Lebanon, https://www.unescwa.org/sites/default/files/pubs/pdf/riccar-main-report-2017-english_0.pdf, 2017.

ESGF: Earth System Grid Federation, https://esgf.github.io, last access: 2 September 2026, 2026a.

ESGF: ESGF MetaGrid, https://metagrid-ceda.east.esgf.io/search, last access: 2 September 2026, 2026b.

Eyring, V., Bony, S., Meehl, G. A., Senior, C. A., Stevens, B., Stouffer, R. J., and Taylor, K. E.: Overview of the Coupled Model Intercomparison Project Phase 6 (CMIP6) experimental design and organization, Geoscientific Model Development, 9, 1937–1958, https://doi.org/10.5194/gmd-9-1937-2016, 2016.

Folk, M., McGrath, R., and Yeager, N.: HDF: an update and future directions, in: IEEE 1999 International Geoscience and Remote Sensing Symposium. IGARSS'99 (Cat. No.99CH36293), vol. 1, pp. 273–275, https://doi.org/10.1109/IGARSS.1999.773469, 1999.

Fox, B., Ramey, C., and contributors: Bash Reference Manual: Reference Documentation for Bash, Free Software Foundation, 5.3 edn., https://www.gnu.org/software/bash/manual/bash.pdf, 2025.

Gelaro, R., McCarty, W., Suárez, M. J., Todling, R., Molod, A., Takacs, L., Randles, C. A., Darmenov, A., Bosilovich, M. G., Reichle, R., Wargan, K., Coy, L., Cullather, R., Draper, C., Akella, S., Buchard, V., Conaty, A., da Silva, A. M., Gu, W., Kim, G.-K., Koster, R., Lucchesi, R., Merkova, D., Nielsen, J. E., Partyka, G., Pawson, S., Putman, W., Rienecker, M., Schubert, S. D., Sienkiewicz, M., and Zhao, B.: The Modern-Era Retrospective Analysis for Research and Applications, Version 2 (MERRA-2), Journal of Climate, 30, 5419–5454, https://doi.org/10.1175/JCLI-D-16-0758.1, 2017.

Giorgi, F., Jones, C., and Asrar, G. R.: Addressing climate information needs at the regional level: the CORDEX framework, World Meteorological Organization (WMO) Bulletin, 58, 175–183, https://wmo.int/media/magazine-article/addressing-climate-information-needs-regional-level-cordex-framework, 2009.

Gutiérrez, J. M., Jones, R. G., Narisma, G. T., Alves, L. M., Amjad, M., Gorodetskaya, I. V., Grose, M., Klutse, N. A. B., Krakovska, S., Li, J., Martínez-Castro, D., Mearns, L. O., Mernild, S. H., Ngo-Duc, T., van den Hurk, B., and Yoon, J.-H.: Atlas, in: Climate Change 2021: The Physical Science Basis. Contribution of Working Group I to the Sixth Assessment Report of the Intergovernmental Panel on Climate Change, edited by Masson-Delmotte, V., Zhai, P., et al., pp. 1927–2058, Cambridge University Press, Cambridge, United Kingdom and New York, NY, USA, https://doi.org/10.1017/9781009157896.021, interactive Atlas available from http://interactive-atlas.ipcc.ch/, 2021.

Gutjahr, O., Putrasahan, D., Lohmann, K., Jungclaus, J. H., von Storch, J.-S., Brüggemann, N., Haak, H., and Stössel, A.: Max Planck Institute Earth System Model (MPI-ESM1.2) for the High-Resolution Model Intercomparison Project (HighResMIP), Geoscientific Model Development, 12, 3241–3281, https://doi.org/10.5194/gmd-12-3241-2019, 2019.

Gutowski Jr., W. J., Giorgi, F., Timbal, B., Frigon, A., Jacob, D., Kang, H.-S., Raghavan, K., Lee, B., Lennard, C., Nikulin, G., O'Rourke, E., Rixen, M., Solman, S., Stephenson, T., and Tangang, F.: WCRP COordinated Regional Downscaling EXperiment (CORDEX): a diagnostic MIP for CMIP6, Geoscientific Model Development, 9, 4087–4095, https://doi.org/10.5194/gmd-9-4087-2016, 2016.

Hanssen-Bauer, I., Førland, E., Haddeland, I., Hisdal, H., Mayer, S., Nesje, A., Nilsen, J., Sandven, S., Sandø, A., Sorteberg, A., Ådlandsvik, B., Andreassen, L., Beldring, S., Bjune, A., Breili, K., Dahl, C. A., Dyrrdal, A., Isaksen, K., Haakenstad, H., Haugen, J., Hygen, H., Langehaug, H., Lauritzen, S.-E., Lawrence, D., Melvold, K., Mezghani, A., Ravndal, O., Risebrobakken, B., Roald, L., Sande, H., Simpson, M., Skagseth, Ø., Skaugen, T., Skogen, M., Støren, E., Tveito, O., and Wong, W.: Klima i Norge 2100: Kunnskapsgrunnlag for klimatilpasning oppdatert i 2015, Report No. 2/2015 (Miljødirektoratet M-406), Norwegian Climate Service Centre (NKSS), Oslo, Norway, https://www.miljodirektoratet.no/publikasjoner/2015/september-2015/klima-i-norge-2100/, 2015.

Harris, C. R., Millman, K. J., van der Walt, S. J., Gommers, R., Virtanen, P., Cournapeau, D., Wieser, E., Taylor, J., Berg, S., Smith, N. J., Kern, R., Picus, M., Hoyer, S., van Kerkwijk, M. H., Brett, M., Haldane, A., del Río, J. F., Wiebe, M., Peterson, P., Gérard-Marchant, P., Sheppard, K., Reddy, T., Weckesser, W., Abbasi, H., Gohlke, C., and Oliphant, T. E.: Array programming with NumPy, Nature, 585, 357–362, https://doi.org/10.1038/s41586-020-2649-2, 2020.

HCLIMcom: HCLIM: HARMONIE-Climate, https://www.hclim.org, last access: 2 September 2026, 2006.

Hersbach, H., Bell, B., Berrisford, P., Hirahara, S., Horányi, A., Muñoz-Sabater, J., Nicolas, J., Peubey, C., Radu, R., Schepers, D., Simmons, A., Soci, C., Abdalla, S., Abellan, X., Balsamo, G., Bechtold, P., Biavati, G., Bidlot, J., Bonavita, M., De Chiara, G., Dahlgren, P., Dee, D., Diamantakis, M., Dragani, R., Flemming, J., Forbes, R., Fuentes, M., Geer, A., Haimberger, L., Healy, S., Hogan, R. J., Hólm, E., Janisková, M., Keeley, S., Laloyaux, P., Lopez, P., Lupu, C., Radnoti, G., de Rosnay, P., Rozum, I., Vamborg, F., Villaume, S., and Thépaut, J.-N.: Complete ERA5 from 1940: Fifth generation of ECMWF atmospheric reanalyses of the global climate, Copernicus Climate Change Service (C3S) Data Store (CDS) [data set], https://doi.org/10.24381/cds.143582cf, 2017.

Hersbach, H., Bell, B., Berrisford, P., Hirahara, S., Horányi, A., Muñoz-Sabater, J., Nicolas, J., Peubey, C., Radu, R., Schepers, D., Simmons, A., Soci, C., Abdalla, S., Abellan, X., Balsamo, G., Bechtold, P., Biavati, G., Bidlot, J., Bonavita, M., De Chiara, G., Dahlgren, P., Dee, D., Diamantakis, M., Dragani, R., Flemming, J., Forbes, R., Fuentes, M., Geer, A., Haimberger, L., Healy, S., Hogan, R. J., Hólm, E., Janisková, M., Keeley, S., Laloyaux, P., Lopez, P., Lupu, C., Radnoti, G., De Rosnay, P., Rozum, I., Vamborg, F., Villaume, S., and Thépaut, J.: The ERA5 global reanalysis, Quarterly Journal of the Royal Meteorological Society, 146, 1999–2049, https://doi.org/10.1002/qj.3803, 2020.

Hofstra, N., Haylock, M., New, M., and Jones, P. D.: Testing E-OBS European high-resolution gridded data set of daily precipitation and surface temperature, Journal of Geophysical Research: Atmospheres, 114, https://doi.org/10.1029/2009JD011799, 2009.

Hunter, J. D.: Matplotlib: A 2D Graphics Environment, Computing in Science & Engineering, 9, 90–95, https://doi.org/10.1109/MCSE.2007.55, 2007.

Hurrell, J. W., Kushnir, Y., Ottersen, G., and Visbeck, M., eds.: The North Atlantic Oscillation: Climatic Significance and Environmental Impact, vol. 134 of *Geophysical Monograph Series*, American Geophysical Union, Washington, DC, https://doi.org/10.1029/GM134, 2003.

Inness, A., Ades, M., Agustí-Panareda, A., Barré, J., Benedictow, A., Blechschmidt, A.-M., Dominguez, J. J., Engelen, R., Eskes, H., Flemming, J., Huijnen, V., Jones, L., Kipling, Z., Massart, S., Parrington, M., Peuch, V.-H., Razinger, M., Remy, S., Schulz, M., and Suttie, M.: The CAMS reanalysis of atmospheric composition, Atmospheric Chemistry and Physics, 19, 3515–3556, https://doi.org/10.5194/acp-19-3515-2019, 2019.

IPCC: Sections, in: Climate Change 2023: Synthesis Report. Contribution of Working Groups I, II and III to the Sixth Assessment Report of the Intergovernmental Panel on Climate Change, edited by Core Writing Team, Lee, H., and Romero, J., pp. 35–115, IPCC, Geneva, Switzerland, https://doi.org/10.59327/IPCC/AR6-9789291691647, 2023.

Jacob, D., Teichmann, C., Sobolowski, S., Katragkou, E., Anders, I., Belda, M., Benestad, R., Boberg, F., Buonomo, E., Cardoso, R. M., Casanueva, A., Christensen, O. B., Christensen, J. H., Coppola, E., De Cruz, L., Davin, E. L., Dobler, A., Domínguez, M., Fealy, R., Fernandez, J., Gaertner, M. A., García-Díez, M., Giorgi, F., Gobiet, A., Goergen, K., Gómez-Navarro, J. J., Alemán, J. J. G., Gutiérrez, C., Gutiérrez, J. M., Güttler, I., Haensler, A., Halenka, T., Jerez, S., Jiménez-Guerrero, P., Jones, R. G., Keuler, K., Kjellström, E., Knist, S., Kotlarski, S., Maraun, D., van Meijgaard, E., Mercogliano, P., Montávez, J. P., Navarra, A., Nikulin, G., de Noblet-Ducoudré, N., Panitz, H.-J., Pfeifer, S., Piazza, M., Pichelli, E., Pietikäinen, J.-P., Prein, A. F., Preuschmann, S., Rechid, D., Rockel, B., Romera, R., Sánchez, E., Sieck, K., Soares, P. M. M., Somot, S., Srnec, L., Sørland, S. L., Termonia, P., Truhetz, H., Vautard, R., Warrach-Sagi, K., and Wulfmeyer, V.: Regional climate downscaling over Europe: perspectives from the EURO-CORDEX community, Regional Environmental Change, 20, 51, https://doi.org/10.1007/s10113-020-01606-9, 2020.

Jones, C., Giorgi, F., and Asrar, G.: The Coordinated Regional Downscaling Experiment: CORDEX, an International Downscaling Link to CMIP5, CLIVAR Exchanges, 16, 34–40, https://www.clivar.org/sites/default/files/documents/Exchanges56.pdf, 2011.

Katragkou, E., Sobolowski, S. P., Teichmann, C., Solmon, F., Pavlidis, V., Rechid, D., Hoffmann, P., Fernandez, J., Nikulin, G., and Jacob, D.: Delivering an Improved Framework for the New Generation of CMIP6-Driven EURO-CORDEX Regional Climate Simulations, Bulletin of the American Meteorological Society, 105, E962–E974, https://doi.org/10.1175/BAMS-D-23-0131.1, 2024.

Kjellström, E., Nikulin, G., Hansson, U., Strandberg, G., and Ullerstig, A.: 21st century changes in the European climate: uncertainties derived from an ensemble of regional climate model simulations, Tellus A: Dynamic Meteorology and Oceanography, 63, 24–40, https://doi.org/10.1111/j.1600-0870.2010.00475.x, 2011.

Kotlarski, S., Keuler, K., Christensen, O. B., Colette, A., Déqué, M., Gobiet, A., Goergen, K., Jacob, D., Lüthi, D., Van Meijgaard, E., Nikulin, G., Schär, C., Teichmann, C., Vautard, R., Warrach-Sagi, K., and Wulfmeyer, V.: Regional climate modeling on European scales: a joint standard evaluation of the EURO-CORDEX RCM ensemble, Geoscientific Model Development, 7, 1297–1333, https://doi.org/10.5194/gmd-7-1297-2014, 2014.

Kuma, P.: Code for the manuscript "EURO-CORDEX-CMIP6 ensemble generated by HCLIM43-ALADIN", GitHub [code], https://github.com/peterkuma/euro-cordex-cmip6-hclim, last access: 19 February 2026, 2026a.

Kuma, P.: Code for the manuscript "EURO-CORDEX-CMIP6 ensemble generated by HCLIM43-ALADIN", version 1.0.0, Zenodo [code], https://doi.org/10.5281/zenodo.22813911, 2026b.

Le Moigne, P., Boone, A., Calvet, J.-C., Decharme, B., Faroux, S., Gibelin, A.-L., Lafont, S., Martin, E., and Masson, V.: SURFEX Scientific Documentation, https://www.umr-cnrm.fr/surfex/, last access: 14 January 2026, 2018.

Le Moigne, P., Bazile, E., Glinton, M., and Verrelle, A.: Documentation of the CERRA-Land system, Report C3S_D322_Lot1.1.1.12_202110_documentation_CERRA-Land, Copernicus Climate Change Service (C3S), https://dast.copernicus-climate.eu/documents/reanalysis-cerra/D322_Lot1.1.1.12_Documentation_CERRA-Land.pdf, 2021.

Lind, P., Lindstedt, D., Kjellström, E., and Jones, C.: Spatial and Temporal Characteristics of Summer Precipitation over Central Europe in a Suite of High-Resolution Climate Models, Journal of Climate, 29, 3501–3518, https://doi.org/10.1175/JCLI-D-15-0463.1, 2016.

Lind, P., Belušić, D., Christensen, O. B., Dobler, A., Kjellström, E., Landgren, O., Lindstedt, D., Matte, D., Pedersen, R. A., Toivonen, E., and Wang, F.: Benefits and added value of convection-permitting climate modeling over Fenno-Scandinavia, Climate Dynamics, 55, 1893–1912, https://doi.org/10.1007/s00382-020-05359-3, 2020.

Lind, P., Belušić, D., Médus, E., Dobler, A., Pedersen, R. A., Wang, F., Matte, D., Kjellström, E., Landgren, O., Lindstedt, D., Christensen, O. B., and Christensen, J. H.: Climate change information over Fenno-Scandinavia produced with a convection-permitting climate model, Climate Dynamics, 61, 519–541, https://doi.org/10.1007/s00382-022-06589-3, 2023.

Lindstedt, D., Lind, P., Kjellström, E., and Jones, C.: A new regional climate model operating at the meso-gamma scale: performance over Europe, Tellus A: Dynamic Meteorology and Oceanography, 67, 24 138, https://doi.org/10.3402/tellusa.v67.24138, 2015.

Lopez, P.: Implementation and validation of a new prognostic large-scale cloud and precipitation scheme for climate and data-assimilation purposes, Quarterly Journal of the Royal Meteorological Society, 128, 229–257, https://doi.org/10.1256/00359000260498879, 2002.

Mascart, P., Bougeault, P., Bechtold, P., Belair, S., Bougeault, P., Carrière, J., Cuxart, J., Ducrocq, V., Fischer, C., Georgelin, M., Héreil, P., Lafore, J., Liousse, C., Mari, C., Mallet, I., Mascart, P., Masson, V., Pinty, J., Richard, E., Suhre, K., Stein, J., Tulet, P., and de Arellano, J. V.-G.: The Meso-NH Atmospheric Simulation System: Scientific Documentation. Part III: Physics, Report, Météo-France and C.N.R.S., Toulouse, France, http://mesonh.aero.obs-mip.fr/mesonh/dir_doc/book1_m48_19jan2009/scidoc_p3.pdf, meso-NH Masdev4.8, 2009.

Masson, V.: A Physically-Based Scheme for the Urban Energy Budget in Atmospheric Models, Boundary-Layer Meteorology, 94, 357–397, https://doi.org/10.1023/A:1002463829265, 2000.

Masson, V., Le Moigne, P., Martin, E., Faroux, S., Alias, A., Alkama, R., Belamari, S., Barbu, A., Boone, A., Bouyssel, F., Brousseau, P., Brun, E., Calvet, J.-C., Carrer, D., Decharme, B., Delire, C., Donier, S., Essaouini, K., Gibelin, A.-L., Giordani, H., Habets, F., Jidane, M., Kerdraon, G., Kourzeneva, E., Lafaysse, M., Lafont, S., Lebeaupin Brossier, C., Lemonsu, A., Mahfouf, J.-F., Marguinaud, P., Mokhtari, M., Morin, S., Pigeon, G., Salgado, R., Seity, Y., Taillefer, F., Tanguy, G., Tulet, P., Vincendon, B., Vionnet, V., and Voldoire, A.: The SURFEXv7.2 land and ocean surface platform for coupled or offline simulation of earth surface variables and fluxes, Geoscientific Model Development, 6, 929–960, https://doi.org/10.5194/gmd-6-929-2013, 2013.

Masson-Delmotte, V., Zhai, P., Pörtner, H.-O., Roberts, D., Skea, J., Shukla, P. R., Pirani, A., Moufouma-Okia, W., Péan, C., Pidcock, R., Connors, S., Matthews, J. B. R., Chen, Y., Zhou, X., Gomis, M. I., Lonnoy, E., Maycock, T., Tignor, M., and Waterfield, T., eds.: Global warming of 1.5°C. An IPCC Special Report on the impacts of global warming of 1.5°C above pre-industrial levels and related global greenhouse gas emission pathways, in the context of strengthening the global response to the threat of climate change, sustainable development, and efforts to eradicate poverty, Cambridge University Press, Cambridge, UK and New York, NY, USA, https://doi.org/10.1017/9781009157940, 2018.

Médus, E., Thomassen, E. D., Belušić, D., Lind, P., Berg, P., Christensen, J. H., Christensen, O. B., Dobler, A., Kjellström, E., Olsson, J., and Yang, W.: Characteristics of precipitation extremes over the Nordic region: added value of convection-permitting modeling, Natural Hazards and Earth System Sciences, 22, 693–711, https://doi.org/10.5194/nhess-22-693-2022, 2022.

Meinshausen, M., Vogel, E., Nauels, A., Lorbacher, K., Meinshausen, N., Etheridge, D. M., Fraser, P. J., Montzka, S. A., Rayner, P. J., Trudinger, C. M., Krummel, P. B., Beyerle, U., Canadell, J. G., Daniel, J. S., Enting, I. G., Law, R. M., Lunder, C. R., O'Doherty, S., Prinn, R. G., Reimann, S., Rubino, M., Velders, G. J. M., Vollmer, M. K., Wang, R. H. J., and Weiss, R.: Historical greenhouse gas concentrations for climate modelling (CMIP6), Geoscientific Model Development, 10, 2057–2116, https://doi.org/10.5194/gmd-10-2057-2017, 2017.

Meinshausen, M., Nicholls, Z. R. J., Lewis, J., Gidden, M. J., Vogel, E., Freund, M., Beyerle, U., Gessner, C., Nauels, A., Bauer, N., Canadell, J. G., Daniel, J. S., John, A., Krummel, P. B., Luderer, G., Meinshausen, N., Montzka, S. A., Rayner, P. J., Reimann, S., Smith, S. J., van den Berg, M., Velders, G. J. M., Vollmer, M. K., and Wang, R. H. J.: The shared socio-economic pathway (SSP) greenhouse gas concentrations and their extensions to 2500, Geoscientific Model Development, 13, 3571–3605, https://doi.org/10.5194/gmd-13-3571-2020, 2020.

Met Office: Cartopy: a cartographic python library with a Matplotlib interface [code], Exeter, Devon, https://cartopy.readthedocs.io/stable/, last access: 2 September 2026, 2010.

MeteoSwiss and ETH Zurich: Climate CH2025 – Scientific Report, Report, Federal Office of Meteorology and Climatology MeteoSwiss, Zurich, Switzerland, https://doi.org/10.18751/climate/scenarios/ch2025/sr/1.0/, 2025.

Mironov, D., Heise, E., Kourzeneva, E., Ritter, B., Schneider, N., and Terzhevik, A.: Implementation of the lake parameterisation scheme FLake into the numerical weather prediction model COSMO, Boreal Environment Research, 15, 218–230, https://www.borenv.net/BER/archive/pdfs/ber15/ber15-218.pdf, 2010.

Nabat, P., Somot, S., Boé, J., Corre, L., Katragkou, E., Li, S., Mallet, M., Meijgaard, E. v., Pavlidis, V., Pietikäinen, J.-P., Sørland, S., and Solmon, F.: Multi-model assessment of the role of anthropogenic aerosols in summertime climate change in Europe, Geophysical Research Letters, https://doi.org/10.1029/2024GL112474, 2025.

Nikulin, G., Jones, C., Giorgi, F., Asrar, G., Büchner, M., Cerezo-Mota, R., Christensen, O. B., Déqué, M., Fernandez, J., Hänsler, A., van Meijgaard, E., Samuelsson, P., Sylla, M. B., and Sushama, L.: Precipitation Climatology in an Ensemble of CORDEX-Africa Regional Climate Simulations, Journal of Climate, 25, 6057–6078, https://doi.org/10.1175/JCLI-D-11-00375.1, 2012.

Noilhan, J. and Planton, S.: A Simple Parameterization of Land Surface Processes for Meteorological Models, Monthly Weather Review, 117, 536–549, https://doi.org/10.1175/1520-0493(1989)117<0536:ASPOLS>2.0.CO;2, 1989.

Nunez, M. and Oke, T. R.: The Energy Balance of an Urban Canyon, Journal of Applied Meteorology and Climatology, 16, 11–19, https://doi.org/10.1175/1520-0450(1977)016<0011:TEBOAU>2.0.CO;2, 1977.

Pichelli, E., Coppola, E., Sobolowski, S., Ban, N., Giorgi, F., Stocchi, P., Alias, A., Belušić, D., Berthou, S., Caillaud, C., Cardoso, R. M., Chan, S., Christensen, O. B., Dobler, A., de Vries, H., Goergen, K., Kendon, E. J., Keuler, K., Lenderink, G., Lorenz, T., Mishra, A. N., Panitz, H.-J., Schär, C., Soares, P. M. M., Truhetz, H., and Vergara-Temprado, J.: The first multi-model ensemble of regional climate simulations at kilometer-scale resolution part 2: historical and future simulations of precipitation, Climate Dynamics, 56, 3581–3602, https://doi.org/10.1007/s00382-021-05657-4, 2021.

Rana, A., Nikulin, G., Kjellström, E., Strandberg, G., Kupiainen, M., Hansson, U., and Kolax, M.: Contrasting regional and global climate simulations over South Asia, Climate Dynamics, 54, 2883–2901, https://doi.org/10.1007/s00382-020-05146-0, 2020.

Rew, R. and Davis, G.: NetCDF: an interface for scientific data access, IEEE Computer Graphics and Applications, 10, 76–82, https://doi.org/10.1109/38.56302, 1990.

Ridal, M., Bazile, E., Le Moigne, P., Randriamampianina, R., Schimanke, S., Andrae, U., Berggren, L., Brousseau, P., Dahlgren, P., Edvinsson, L., El-Said, A., Glinton, M., Hagelin, S., Hopsch, S., Isaksson, L., Medeiros, P., Olsson, E., Unden, P., and Wang, Z. Q.: CERRA, the Copernicus European Regional Reanalysis system, Quarterly Journal of the Royal Meteorological Society, 150, 3385–3411, https://doi.org/10.1002/qj.4764, 2024.

Roberts, M. J. et al.: The Benefits of Global High-Resolution for Climate Simulation: Process Understanding and the Enabling of Stakeholder Decisions at the Regional Scale, Bulletin of the American Meteorological Society, 99, 2341–2359, https://doi.org/10.1175/BAMS-D-15-00320.1, 2018.

Samuelsson, P., Gollvik, S., Jansson, C., Kupiainen, M., Kourzeneva, E., and van de Berg, W. J.: The Surface Processes of the Rossby Centre Regional Atmospheric Climate Model (RCA4), Report in Meteorology No. 157, Swedish Meteorological and Hydrological Institute (SMHI), Norrköping, Sweden, https://www.smhi.se/download/18.6ae791dc18fc9e7539e1cd19/1717701182868/Meteorologi_157%20The%20surface%20processes%20of%20the%20Rossby%20Centre%20regional%20atmospheric%20climate%20model%20(RCA4).pdf, 2015.

Schilliger, L., Wild, M., Fischer, E. M., and Seneviratne, S. I.: An Investigation on Causes of the Detected Surface Solar Radiation Trends Over Europe, Journal of Geophysical Research: Atmospheres, 129, e2024JD041 101, https://doi.org/10.1029/2024JD041101, 2024.

Schimanke, S., Ridal, M., Le Moigne, P., Berggren, L., Undén, P., Randriamampianina, R., Andrea, U., Bazile, E., Bertelsen, A., Brousseau, P., Dahlgren, P., Edvinsson, L., El Said, A., Glinton, M., Hopsch, S., Isaksson, L., Mladek, R., Olsson, E., Verrelle, A., and Wang, Z. Q.: CERRA sub-daily regional reanalysis data for Europe on single levels from 1984 to present, Copernicus Climate Change Service (C3S) Climate Data Store (CDS) [data set], https://doi.org/10.24381/cds.622a565a, 2021.

Schulzweida, U.: CDO User Guide, 2.3.0 edn., https://doi.org/10.5281/zenodo.10020800, 2023.

Schumacher, D. L., Singh, J., Hauser, M., Fischer, E. M., Wild, M., and Seneviratne, S. I.: Exacerbated summer European warming not captured by climate models neglecting long-term aerosol changes, Communications Earth & Environment, 5, 182, https://doi.org/10.1038/s43247-024-01332-8, 2024.

Seland, Ø., Bentsen, M., Olivié, D., Toniazzo, T., Gjermundsen, A., Graff, L. S., Debernard, J. B., Gupta, A. K., He, Y.-C., Kirkevåg, A., Schwinger, J., Tjiputra, J., Aas, K. S., Bethke, I., Fan, Y., Griesfeller, J., Grini, A., Guo, C., Ilicak, M., Karset, I. H. H., Landgren, O., Liakka, J., Moseid, K. O., Nummelin, A., Spensberger, C., Tang, H., Zhang, Z., Heinze, C., Iversen, T., and Schulz, M.: Overview of the Norwegian Earth System Model (NorESM2) and key climate response of CMIP6 DECK, historical, and scenario simulations, Geoscientific Model Development, 13, 6165–6200, https://doi.org/10.5194/gmd-13-6165-2020, 2020.

Sobolowski, S., Somot, S., Fernandez, J., Evin, G., Brands, S., Maraun, D., Kotlarski, S., Jury, M., Benestad, R. E., Teichmann, C., Christensen, O. B., Bülow, K., Buonomo, E., Katragkou, E., Steger, C., Sørland, S., Nikulin, G., McSweeney, C., Dobler, A., Palmer, T., Wilcke, R., Boé, J., Brunner, L., Ribes, A., Qasmi, S., Nabat, P., Sevault, F., and Oudar, T.: GCM Selection & Ensemble Design: Best Practices and Recommendations from the EURO-CORDEX Community, Bulletin of the American Meteorological Society, 106, E1834–E1850, https://doi.org/10.1175/BAMS-D-23-0189.1, 2025.

Stallman, R. M.: The GNU Manifesto, https://archive.org/details/dr_dobbs_journal_vol_10/, 1985.

Strandberg, G., Bärring, L., Hansson, U., Jansson, C., Jones, C., Kjellström, E., Kolax, M., Kupiainen, M., Nikulin, G., Samuelsson, P., Ullerstig, A., and Wang, S.: CORDEX scenarios for Europe from the Rossby Centre regional climate model RCA4, Report in Meteorology and Climatology No. 116, Swedish Meteorological and Hydrological Institute (SMHI), Norrköping, Sweden, https://www.smhi.se/download/18.38e7941719209b36a1fb1ed/1728367246648/RMK_116.pdf, 2015.

Séférian, R., Nabat, P., Michou, M., Saint-Martin, D., Voldoire, A., Colin, J., Decharme, B., Delire, C., Berthet, S., Chevallier, M., Sénési, S., Franchisteguy, L., Vial, J., Mallet, M., Joetzjer, E., Geoffroy, O., Guérémy, J.-F., Moine, M.-P., Msadek, R., Ribes, A., Rocher, M., Roehrig, R., Salas-y Mélia, D., Sanchez, E., Terray, L., Valcke, S., Waldman, R., Aumont, O., Bopp, L., Deshayes, J., Éthé, C., and Madec, G.: Evaluation of CNRM Earth System Model, CNRM-ESM2-1: Role of Earth System Processes in Present-Day and Future Climate, Journal of Advances in Modeling Earth Systems, 11, 4182–4227, https://doi.org/10.1029/2019MS001791, 2019.

Tange, O.: GNU parallel: The Command-Line Power tool, The USENIX Magazine, 36, 42–47, https://www.usenix.org/system/files/login/articles/105438-Tange.pdf, 2011.

Tatebe, H., Ogura, T., Nitta, T., Komuro, Y., Ogochi, K., Takemura, T., Sudo, K., Sekiguchi, M., Abe, M., Saito, F., Chikira, M., Watanabe, S., Mori, M., Hirota, N., Kawatani, Y., Mochizuki, T., Yoshimura, K., Takata, K., O'ishi, R., Yamazaki, D., Suzuki, T., Kurogi, M., Kataoka, T., Watanabe, M., and Kimoto, M.: Description and basic evaluation of simulated mean state, internal variability, and climate sensitivity in MIROC6, Geoscientific Model Development, 12, 2727–2765, https://doi.org/10.5194/gmd-12-2727-2019, 2019.

Taylor, K. E., Stouffer, R. J., and Meehl, G. A.: An Overview of CMIP5 and the Experiment Design, Bulletin of the American Meteorological Society, 93, 485–498, https://doi.org/10.1175/BAMS-D-11-00094.1, 2012.

Taylor, K. E., Juckes, M., Balaji, V., Cinquini, L., Denvil, S., Durack, P. J., Elkington, M., Guilyardi, E., Kharin, S., Lautenschlager, M., Lawrence, B., Nadeau, D., and Stockhause, M.: CMIP6 Model Output Metadata Requirements, Data Reference Syntax (DRS) and Controlled Vocabularies (CVs), https://doi.org/10.5281/zenodo.15670624, version 6.2.8, 2025.

Tegen, I., Hollrig, P., Chin, M., Fung, I., Jacob, D., and Penner, J.: Contribution of different aerosol species to the global aerosol extinction optical thickness: Estimates from model results, Journal of Geophysical Research: Atmospheres, 102, 23 895–23 915, https://doi.org/10.1029/97JD01864, 1997.

Termonia, P., Fischer, C., Bazile, E., Bouyssel, F., Brožková, R., Bénard, P., Bochenek, B., Degrauwe, D., Derková, M., El Khatib, R., Hamdi, R., Mašek, J., Pottier, P., Pristov, N., Seity, Y., Smolíková, P., Španiel, O., Tudor, M., Wang, Y., Wittmann, C., and Joly, A.: The ALADIN System and its canonical model configurations AROME CY41T1 and ALARO CY40T1, Geoscientific Model Development, 11, 257–281, https://doi.org/10.5194/gmd-11-257-2018, 2018.

Torvalds, L.: Linux: a portable operating system, Master's thesis, University of Helsinki, Helsinki, Finland, https://www.cs.helsinki.fi/u/kutvonen/index_files/linus.pdf, 1997.

UERRA: Uncertainties in Ensembles of Regional ReAnalyses, https://www.uerra.eu, last access: 9 September 2026, 2026.

UERRA, Copernicus Climate Change Service, and ECA&D: E-OBS data access, Copernicus Climate Change Service (C3S) [data set], https://surfobs.climate.copernicus.eu/dataaccess/access_eobs.php, last access: 9 September 2026, 2026.

van der Schrier, G., van den Besselaar, E. J. M., Klein Tank, A. M. G., and Verver, G.: Monitoring European average temperature based on the E-OBS gridded data set, Journal of Geophysical Research: Atmospheres, 118, 5120–5135, https://doi.org/10.1002/jgrd.50444, 2013.

van Lipzig, N. P. M., Van de Walle, J., Belušić, D., Berthou, S., Coppola, E., Demuzere, M., Fink, A. H., Finney, D. L., Glazer, R., Ludwig, P., Marsham, J. H., Nikulin, G., Pinto, J. G., Rowell, D. P., Wu, M., and Thiery, W.: Representation of precipitation and top-of-atmosphere radiation in a multi-model convection-permitting ensemble for the Lake Victoria Basin (East-Africa), Climate Dynamics, 60, 4033–4054, https://doi.org/10.1007/s00382-022-06541-5, 2022.

Van Rossum, G.: An introduction to Python, Network Theory Ltd. Bristol, 15 Royal Park, Clifton, Bristol BS8 3AL, United Kingdom, 2003.

van Ulden, A., Lenderink, G., van den Hurk, B., and van Meijgaard, E.: Circulation Statistics and Climate Change in Central Europe: PRUDENCE Simulations and Observations, Climatic Change, 81, 179–192, https://doi.org/10.1007/s10584-006-9212-5, 2007.

van Vuuren, D. P., Riahi, K., Calvin, K., Dellink, R., Emmerling, J., Fujimori, S., KC, S., Kriegler, E., and O'Neill, B.: The Shared Socio-economic Pathways: Trajectories for human development and global environmental change, Global Environmental Change, 42, 148–152, https://doi.org/10.1016/j.gloenvcha.2016.10.009, 2017.

Vautard, R., Kadygrov, N., Iles, C., Boberg, F., Buonomo, E., Bülow, K., Coppola, E., Corre, L., van Meijgaard, E., Nogherotto, R., Sandstad, M., Schwingshackl, C., Somot, S., Aalbers, E., Christensen, O. B., Ciarlo, J. M., Demory, M.-E., Giorgi, F., Jacob, D., Jones, R. G., Keuler, K., Kjellström, E., Lenderink, G., Levavasseur, G., Nikulin, G., Sillmann, J., Solidoro, C., Sørland, S. L., Steger, C., Teichmann, C., Warrach-Sagi, K., and Wulfmeyer, V.: Evaluation of the Large EURO-CORDEX Regional Climate Model Ensemble, Journal of Geophysical Research: Atmospheres, 126, e2019JD032 344, https://doi.org/10.1029/2019JD032344, 2021.

Verrelle, A., Glinton, M., Bazile, E., Le Moigne, P., Randriamampianina, R., Ridal, M., Berggren, L., Undén, P., Schimanke, S., Mladek, R., and Soci, C.: CERRA-Land sub-daily regional reanalysis data for Europe from 1984 to present, Copernicus Climate Change Service (C3S) Climate Data Store (CDS) [data set], https://doi.org/10.24381/cds.a7f3cd0b, 2022.

Virtanen, P., Gommers, R., Oliphant, T. E., Haberland, M., Reddy, T., Cournapeau, D., Burovski, E., Peterson, P., Weckesser, W., Bright, J., van der Walt, S. J., Brett, M., Wilson, J., Millman, K. J., Mayorov, N., Nelson, A. R. J., Jones, E., Kern, R., Larson, E., Carey, C. J., Polat, İ., Feng, Y., Moore, E. W., VanderPlas, J., Laxalde, D., Perktold, J., Cimrman, R., Henriksen, I., Quintero, E. A., Harris, C. R., Archibald, A. M., Ribeiro, A. H., Pedregosa, F., van Mulbregt, P., Vijaykumar, A., Bardelli, A. P., Rothberg, A., Hilboll, A., Kloeckner, A., Scopatz, A., Lee, A., Rokem, A., Woods, C. N., Fulton, C., Masson, C., Häggström, C., Fitzgerald, C., Nicholson, D. A., Hagen, D. R., Pasechnik, D. V., Olivetti, E., Martin, E., Wieser, E., Silva, F., Lenders, F., Wilhelm, F., Young, G., Price, G. A., Ingold, G.-L., Allen, G. E., Lee, G. R., Audren, H., Probst, I., Dietrich, J. P., Silterra, J., Webber, J. T., Slavič, J., Nothman, J., Buchner, J., Kulick, J., Schönberger, J. L., de Miranda Cardoso, J. V., Reimer, J., Harrington, J., Rodríguez, J. L. C., Nunez-Iglesias, J., Kuczynski, J., Tritz, K., Thoma, M., Newville, M., Kümmerer, M., Bolingbroke, M., Tartre, M., Pak, M., Smith, N. J., Nowaczyk, N., Shebanov, N., Pavlyk, O., Brodtkorb, P. A., Lee, P., McGibbon, R. T., Feldbauer, R., Lewis, S., Tygier, S., Sievert, S., Vigna, S., Peterson, S., More, S., Pudlik, T., Oshima, T., Pingel, T. J., Robitaille, T. P., Spura, T., Jones, T. R., Cera, T., Leslie, T., Zito, T., Krauss, T., Upadhyay, U., Halchenko, Y. O., and and, Y. V.-B.: SciPy 1.0: fundamental algorithms for scientific computing in Python, Nature Methods, 17, 261–272, https://doi.org/10.1038/s41592-019-0686-2, 2020.

Wang, F., Belušić, D., Amorim, J. H., and Ribeiro, I.: Assessing the impacts of physiography refinement on Stockholm summer urban temperature simulated with an offline land surface model, Urban Climate, 49, 101 531, https://doi.org/10.1016/j.uclim.2023.101531, 2023.

Whitaker, J. and contributors: pyproj Documentation, 3.7.2 edn., https://pyproj4.github.io/pyproj/stable/, 2026.

WMO: Seventeenth World Meteorological Congress: Abridged Final Report with Resolutions, Report WMO-No. 1157, World Meteorological Organization, Geneva, Switzerland, https://library.wmo.int/idurl/4/54771, 2015.

Wu, M., Nikulin, G., Kjellström, E., Belušić, D., Jones, C., and Lindstedt, D.: The impact of regional climate model formulation and resolution on simulated precipitation in Africa, Earth System Dynamics, 11, 377–394, https://doi.org/10.5194/esd-11-377-2020, 2020.

Yeste, P., Domínguez, M., Senent-Aparicio, J., Andreu, J., and Pulido-Velazquez, M.: Projected hydrologic changes over the headwater areas of the Duero River Basin using Euro-CORDEX regional climate simulations, Science of The Total Environment, 777, 146 126, https://doi.org/10.1016/j.scitotenv.2021.146126, 2021.